國立臺灣大學生命科學院分子與細胞生物學研究所

碩士論文

Institute of Molecular and Cellular Biology
College of Life Science
National Taiwan University
Master Thesis

Terc(−/−)模式小鼠的退化病徵研究

Characterization of the degenerative phenotype of a *Terc*(−/−) animal model

曾宛儀
Wan-Yi Tzeng

指導教授: 朱雪萍 博士、陳律佑 博士

Advisor: Hsueh-Ping Chu, Ph.D., Liuh-Yow Chen, Ph.D.

中華民國 112 年 5 月
May 2023

doi:10.6342/NTU202301366

國立臺灣大學碩士學位論文口試委員會審定書

國立臺灣大學碩士學位論文
口試委員會審定書
MASTER'S THESIS ACCEPTANCE CERTIFICATE
NATIONAL TAIWAN UNIVERSITY

Terc(−/−)模式小鼠的退化病徵研究

Characterization of the degenerative phenotype of a *Terc*(−/−) animal model

本論文係 曾宛儀(R09B43040) 在國立臺灣大學 分子與細胞生物學研究所 完成之碩士學位論文，於民國 112 年 5 月 23 日承下列考試委員審查通過及口試及格，特此證明。

The undersigned, appointed by the Department / Institute of Molecular and Cellular Biology on 23 May, 2023 have examined a Master's thesis entitled above presented by Tzeng, Wan-yi (R09b43040) candidate and hereby certify that it is worthy of acceptance.

口試委員 Oral examination committee:

（指導教授 Advisor）

系主任/所長 Director:

doi:10.6342/NTU202301366

誌謝

很感激在碩班的過程中，獲得了許多人的幫助與教導，才得以將這篇論文順利完成。感謝中研院 分生所 陳律佑老師一開始排除萬難讓我能在他的指導下學習，在碩班的過程中，提供我非常開明且完善的研究環境，讓我能自由的做各種多樣有趣的實驗; 並且不厭其煩地在實驗上與生活上給予我方向以及協助。除了論文本身研究內容，也給我很多機會接觸不一樣的實驗與研究討論。

以及台大 分細所 朱雪萍老師，即便我較少參與實驗室的研究，仍然待我如其他同學一般，非常有耐心，並且不吝嗇在我遇到困難時提供協助與建議，也讓我不在校園的生活，得到很多便利與照顧。

感謝 IMB R421 與 NTU 807 的研究成員們，給了我很多實驗上的建議與幫助，在每次的實驗進度報告中點出需要加強的部分，讓我的口語表達能力與邏輯架構都日漸進步，也在日常生活中陪伴我一起度過這些充實的日子。另外，也感謝 IMB 核心設施(動物房、顯微鏡影像設施室、流式細胞分析室)的學長姐們，提供了我非常多實驗上的專業支援，讓我能夠得到許多精準的分析結果以及漂亮的實驗影像。

最後感謝家人朋友與愛我的人們，給予我需要的陪伴，並且承接那些無法自己消化的負面情緒。義無反顧地用數不盡的耐心與包容陪伴我度過這段期間。謝謝這一路上給我支持與協助的所有人，讓我能勇敢完成一個個艱難的挑戰。也謝謝自己在面對無數個挫折的時刻，仍堅持到今天。在未來的日子裡我會將這些溫柔銘記在心，謝謝每一個人的支持與參與。

2023.7.5 曾宛儀

doi:10.6342/NTU202301366

摘要

端粒長度與細胞衰老已被證實與多種衰老疾病有高度相關。端粒酶複合物（Telomerase complex）能在特定細胞類型中維持端粒長度並保護染色體完整性，而其中端粒酶的 RNA 成分 *Terc*（也稱為 TR）含有端粒序列合成的模板。先前的研究顯示，在小鼠中，*Terc* 缺失引起會多種衰老表型，其中包括生殖缺陷。在端粒酶基因剔除小鼠後代中，隨著端粒持續的短化，*Terc* 剔除小鼠繁殖至第六代(G6)便無法生育。

目前，在端粒相關的老化動物模型中，需花費大量的時間繁殖端粒酶功能缺失的後代。因此，本研究的目的是建立在較年輕以及前期世代便能進行老化實驗的端粒缺失動物模型。在本研究中，我們使用先前研究所使用的同一品系 *Terc* 缺失小鼠(JAX stock #004132)與本地野生型 C57BL/6 品系進行交配，以獲得異質性 *Terc* 小鼠，並進一步繁殖 *Terc* 缺失子代（t*Terc*），發現由此繁殖的 t*Terc* 品系僅能繁殖到第三代 (G3)。我們推測是因為本地野生型 C57BL/6J 小鼠的端粒長度較短，因而繁殖出端粒較短且無法維持的 t*Terc* 小鼠。我們進一步針對 t*Terc* 小鼠進行老化程度表徵和基礎生理參數檢測，包括外觀、組織學以及血液學分析。在結果中，我們觀察到 6 個月和 9 個月的 G2 t*Terc* 小鼠中，各種器官（如肺、腸道和生殖器官）的退化表現。

在外觀變化中，體重積累率在 t*Terc* 提前下降。另外透過組織切片觀察到 G2 t*Terc* 小鼠體內高度增殖器官（如生殖器官和腸道隱窩）受損，進而造成生殖能力下降，無法產生 G3 後代。而器官的受損引發體內發炎現象與相關症狀在周邊血液分析得到證實。除此之外，我們使用 G2 t*Terc* 小鼠與異質性 *Terc* 小鼠交配以獲得 G3 t*Terc*(iG3)和異質性 *Terc* 小鼠，並分析 iG3 脾臟內血球組成，結果亦顯示端粒酶缺失會造成血球比例變化。

在本研究中，我們使用組織學、血液學和生理學研究對端粒酶缺失小鼠的 t*Terc* 品系進行了表徵分析，並證明了 t*Terc* 模式動物中 *Terc* 缺失會引起不正常衰老與發炎，其中包含: (1)產生 G3 的生殖能力顯著下降 (p-value = 0.0047); (2)提前出現體重增長停滯; (3)生殖細胞生長障礙; (4)小腸隱窩數量減少; (5)周邊血液組成變化; 以及(6) iG3 中脾臟白血球變化。這些結果顯示 t*Terc* 小鼠與先前的端粒酶缺失品系中，提前展現了退化表現。而在未來相關的端粒研究中，t*Terc* 模型能加速生成

doi:10.6342/NTU202301366

端粒缺失的小鼠模型，將此模式動物應用於多種與衰老相關的疾病。包含促進藥物開發、臨床應用，甚至是癌症治療的研究。

關鍵字：端粒、端粒酶、老化、端粒酶 RNA 組分、端粒縮短

doi:10.6342/NTU202301366

Abstract

Telomere length is highly correlated with cellular senescence and several aging-associated diseases. The telomerase complex maintains telomere length and protects chromosome integrity in specific cell types. The RNA component of telomerase *Terc* (also known as TR) contains the template for telomeric sequence synthesis. Previous studies have shown that *Terc* deficiency in mice induces multiple aging phenotypes, including reproductive defects. Along with continuous telomere shortening displayed by the offspring of telomerase knockout mice, *Terc*-deficient mice are infertile by generation six (G6).

Currently, significant time and cost have been expended on generating offspring and studying the effects of telomerase deficiency in aging animal models. Therefore, the aim of this study is to generate a more suitable animal model in both younger age and earlier generations for telomerase research. When the same strain of *Terc*-deletion mice used in above mentioned studies (JAX stock #004132) were crossed it with the local wild type C57BL/6 strain to obtain heterozygous *Terc* mice, which were then crossed to generate *Terc*-deletion progeny (t*Terc*), it was found that the generated t*Terc* strain could only be bred to generation 3 (G3), presumably because of the shorter telomere length of local wild type C57BL/6J mice. Upon characterizing aging progression in wild type and the generated t*Terc* line at G2, as well as basal physiological parameters, including appearance observation, histology and hematology, degenerative phenotypes in various organs, such as lungs, intestine, and sexual organs of 6- and 9-month-old G2 t*Terc* mice were observed.

In the appearance record, we noted that the body weight accumulation rate lost was at an earlier age in G2 tTerc mice. Through histology, we observed that G2 t*Terc* mice showed organ damage in some highly proliferative structures. Additionally, physiological

doi:10.6342/NTU202301366

inflammation symptoms were confirmed by peripheral complete blood count. Furthermore, when we crossed G2 t*Terc* with heterozygous *Terc* mice to acquire inbred G3 t*Terc* (iG3) and heterozygous *Terc*, the analysis of iG3 splenic blood showed changes in blood cell composition in telomerase deficiency mice.

In our study, we characterized the local background strain of telomerase knockout mice using histology, hematology, and physiological measures. We demonstrated that t*Terc* mice exhibit degenerative phenotypes at earlier generations than previous model strains. These include: (1) a significant reduction in reproductive capability to produce G3 (p-value = 0.0047); (2) an earlier arrest of body weight gain; (3) an increase in sexual organ atrophy (6 months of WT vs. G2: 99% vs. 10%, p-value <0.0001); (4) intestinal crypts distortion (9 months of WT vs. G2: 20 vs 11 crypts number/mm, p-value <0.0001); (5) changes in peripheral blood composition; and (6) an increase in granulocytes (p-value = 0.0159) and inflammatory monocytes (p-value = 0.0317), and a decrease in CD8+ T cells (p-value = 0.0159) in the analysis of iG3 splenic blood.

Our thesis presents a novel strategy that accelerates the generation of a valuable mouse model for telomere research. This model can provide fundamental insights into biology and be used to study multiple aging-related diseases. By facilitating the study of drug development, clinical applications, and even cancer therapies, this model has the potential to make significant contributions to the field of telomere research.

Key words: Aging; Telomerase; *Terc*; Telomeres; short telomeres;

doi:10.6342/NTU202301366

Contents

doi:10.6342/NTU202301366

doi:10.6342/NTU202301366

List of Figures

List of Appendix Figures

doi:10.6342/NTU202301366

List of Tables

doi:10.6342/NTU202301366

Chapter 1 Introduction

1. Telomere introduction

1.1 Telomere

Telomeres are repetitive nucleotide (5′-TTAGGG-3′) sequences at the ends of eukaryotic linear chromosomes. Telomeres protect the ends of chromosomes from shortening due to cell division and prevent chromosome end fusion, thus maintaining the integrity of chromosomes [1, 2]. Besides the tandem repeat sequences, chromosome ends also harbor a six-subunit protein complex, Shelterin, that protects the chromosome ends by facilitating the formation of a lariat loop (t-loop) [3]. Additionally, the G-rich 3’ overhang can fall back and invade the double-stranded telomeric region, forming the displacement loop (D-loop).

Each time the cell divides, the telomeres are shortened by 50-200 base pairs (bp)[4] due to the incomplete replication of DNA by DNA polymerases. This phenomenon, known as the end replication problem, leads to the progressive shortening of telomeres. Once telomeres’ length is critically shortened, i.e., crossing the critical threshold, chromosome instability arises, resulting in cellular senescence and eventually apoptosis [5, 6]. Telomere shortening has a crucial role in aging and is related to several age-related diseases. Interestingly, the length of telomeres varies across different species, ages and even cell types. Human telomeres typically range in length from 0.5 to 15 kilobase pairs (kb), while laboratory mice have much longer telomeres around 50 to 150 kb [7, 8].

1.2 Telomerase

Telomerase, a ribonucleoprotein, is responsible for maintaining length of telomeres, by adding the telomere repeat sequence to the 3’ end of the telomere. Fast dividing cells, such as stem cells and cancer cells, have active telomerase [9, 10]. Telomerase is a

doi:10.6342/NTU202301366

specialized reverse transcriptase enzyme composed of two main components – the catalytic protein subunit, known as telomerase reverse transcriptase (TERT), and the telomerase RNA component (*Terc*). TERT is responsible for synthesizing the telomere repeats, while *Terc* serves as the RNA template. The sequence of the RNA template is 3'-CAAUCCCAAUC-5'. When telomerase is active, TERT adds TTAGGG repeats through reverse transcription, using *Terc* as the template. As a result, the telomere DNA sequence is added to the 3' end of telomeres, thus preserving the integrity of the chromosomes.

1.3 Telomere relevant diseases

Telomere length is a prominent biomarker of aging, as it is a defining hallmark of cellular senescence and organismal degeneration. Consequently, telomere shortening is considered to be the onset of several age-associated pathologies, and is even associated with lifespan [11, 12]. Shortening of telomeres, telomere dysfunction and mutations of telomere maintenance genes occurring in different tissues can result in diverse diseases. In humans, premature aging and pathologic features due to telomere dysfunction have been investigated, e.g., cardiomyocyte hypertrophy and fibrosis [13], idiopathic pulmonary fibrosis (IPF) [14-16] and liver cirrhosis [17-19] etc.

The premature loss of the regenerative capacity of tissues is characterized by the presence of short telomeres, affecting tissues with both high and low proliferation rates. Diseases that are related to shortened telomeres are known as telomeropathies [11, 20, 21]. Several stem cell renewal dysfunctions and bone marrow failure also feature shortened telomeres, resulting in syndromes such as dyskeratosis congenita (DC), aplastic anemia and Myelodysplastic syndrome (MDS) etc. [22, 23]. Moreover, telomere length is highly inherited. Shorter telomeres at birth manifests as several severe symptoms in pediatric patients.

doi:10.6342/NTU202301366

The reliance on organ transplantation as a primary treatment option for patients with telomere diseases underscores the urgent need for the development of alternative, more effective therapies that address the underlying genetic abnormalities [21]. The current lack of specific and efficient therapies in clinical practice presents a significant challenge for the management and treatment of these complex and often debilitating genetic disorders.

2. Telomere deficient animal model

Mouse models with genetic modifications in telomerase were developed to study the consequences of telomerase deficiency. The first such animal model was established in the 1990s by deleting the telomerase RNA gene (Terc) in C57BL/6J mice [24, 25]. Heritable progressive telomere shortening limits the number of generations that can be derived from this telomerase activity deficient mouse genotype before complete loss of viability. Deficiency of telomerase in the mouse models results in several phenotypes, including – (i) infertility and embryonic mortality as a result of defective closure of the neural tube; (ii) shorter small intestinal villi and severe intestinal atrophy; (iii) spleen atrophy and lack of B and T lymphocytes; (iv) impaired germinal center function; (v) abnormal angiogenic potential; and (vi) reduced proliferative potential of bone marrow stem cells. These phenotypes provide insight into the role of telomerase in various organ systems and highlight the importance of telomere maintenance in overall health.

The above described phenotypes are derived due to abnormal telomere length, which plays a key role in determining the severity of symptoms. The progression of telomere dysfunction can be evaluated in *Terc* deletion animals from different backgrounds. In previous studies, most *Terc* deletion mouse models can produce progeny up to sixth generation, and exhibit most of the well-known phenotypes from the fourth generation.

doi:10.6342/NTU202301366

3. Study aim

For this study, *Terc* deletion mice were maintained as heterozygous *Terc*, by crossing with the local wild type C57BL/6J mice. Interestingly, subsequently bred t*Terc* animal model obtained by crossing heterozygous *Terc* showed phenotypes with advanced tissue degeneration and decreased litter size compared with the original strain.

In this study, we investigate the consequences of telomerase deficiency in the second generation of t*Terc* mice, and explore the effects of telomere dysfunction. To do so, we measured telomere length in mouse embryonic fibroblast cells (MEF) isolated from G2 embryos. The results of the TRF assay and telomere-FISH showed shorter telomeres in the G2 MEF cells. We then sought to characterize the phenotype in G2 t*Terc* mice by tracking blood components, individual body size, and various organs through histological assessment, including the sexual organs, lung, digestive system, and blood. In addition, to circumvent the reproduction barrier, we generated a third generation (iG3) of homozygous *Terc* deletion mice by crossing G2 t*Terc* with heterozygous mice, and compared the splenic hematopoiesis of homozygous and heterozygous *Terc* mice.

doi:10.6342/NTU202301366

Chapter 2 Results

2.1 Mouse breeding

Telomerase RNA component (*Terc*) deficiency results in lack of telomerase activity, further causing telomere shortening and chromosomal instability in mice of late generations or with age. Moreover, *Terc*$^{-/-}$ animals have risen infertility from the fourth (G4) to sixth (G6) generation[24, 26, 27]. The same strain of *Terc*$^{-/-}$ animal (RRID: IMSR_JAX: 004132) was acquired from *The Jackson laboratory* and crossed with the local wild type strain C57BL/6, with a mixed background. Infertility was observed as early as in the third generation (G3).

To characterize phenotypes of telomere dysfunction, Terc deficiency mice were crossed with local wild type mouse, and the resulting mice with heterozygous *Terc* genotype were designated as G0 (Fig. 1A). G0 heterozygous mice were intercrossed to obtain G1 homozygous (G1 t*Terc*), heterozygous and wild type. Since mouse telomere length is about 50-150 kb, the phenotypes are usually observed in the later generations (between G4 – G6). G1 t*Terc* mice were crossed to produce such mouse models with shorter telomere length. However, unexpectedly the reproductive ability of the G2 t*Terc* mice was also significantly decreased. To confirm if this observed premature features are triggered by telomerase deficiency, G2 t*Terc* was crossed with G0 heterozygous mice to generate homozygous and heterozygous progeny and this mixed background generation is designated as inbred generation 3 (iG3) (Fig. 1A). From the mating records of all generations, a trend of decreasing litter size in each subsequent generation was evident, which indicates that the litter size decreases with the deficiency of telomerase in the offspring (Fig. 1B). Heterozygous intercross mating produced 6 to 13 pups per litter, the produced average is 8.3 pups per litter from total 8 mating. The number was consistent with the studied wild type mouse. However, crossing homozygous deletion mice of the

doi:10.6342/NTU202301366

first generation (G1 t*Terc*), the litter size decreased significantly (*p*-value = 0.0047), the average decline to 5 pups per litter. Besides, the maximum litter size dropped to only 7 G2 t*Terc* pups. Moreover, during the 6-month mating period with G2 t*Terc* mice, only two litters of G3 were produced from 4 mating cages. Notably, these two litters only had 3 pups each – a further decrease in litter size.

Thus, instead of generating G4 to G6 homozygous *Terc* mice for this study, the G2 t*Terc* mice were studied. To this end, the health status of G2 t*Terc* mice were monitored by continuously recording abnormal appearance and body weight before the animals were sacrificed (Fig 1C), and compare with same age of wildtype. The phenotypes of selected organ systems of G2 t*Terc* mice were investigated at 2 individual time points – younger (at 6 months) and older (at 9 months) ages. And the hematology analysis is collected at 3 time points: completely mature age (8 weeks), younger (at 6 months) and older (at 9 months) ages. Based on these different aspects record and analysis to characterize the degenerative phenotype in t*Terc* animals

doi:10.6342/NTU202301366

2.2 Body weight and rate of weight gain

Mice were weaned at 3 weeks, and their body weights were recorded until sacrifice. G2 mice were observed to have lower body weight compared with wild type. Differences in appearance between G2 t*Terc* and wild type control mice were noted by visual observation at 6 months age (Fig. 2A). Similarly, G2 t*Terc* mice consistently weighed lesser than the wild type. Both male and female G2 t*Terc* were smaller in size at weaning age (3 weeks) (Fig. 2B, Table 1). In males, there is 0.27 g lower on average, and in females, much 1.71 g lower on average. Even more, after weaning, significantly lower body weight can be observed starting from 20 weeks age and continuously lower from 29 weeks in males; and in females, significantly lower from 12, and continuously lower until the end of the record. Interestingly, at 36 weeks, the average body weight of male t*Terc* mice was lower than female wild type mice.

In addition, we also consider the weaning weight as base (100%), and calculated the rate of body weight gain in the later weeks. The rate of weight gain was similar in both groups at earlier time points (Table 2). t*Terc* mice had similar weight gain compared to wild type (Fig. 2C). However, after the aforementioned time points, both genders of t*Terc* mice experienced a decrease in body weight gain. Consequently, after the t*Terc* mice stopped gaining weight, body weight was decreased in few weeks. At the end of record (36-weeks), male have 28.26% difference between tTerc and wildtype, and 25.51% in female.

We speculated that the telomere dysfunction in t*Terc* mice affects the proliferation of highly regenerative cells with age, like the digestive system, which leads to hypoplasia or inflammation, and might contribute to impaired nutrient absorption.

2.3 Telomere length

doi:10.6342/NTU202301366

To investigate the relationship between telomerase deficiency and degenerative phenotype, telomere length was directly measured by telomere restriction fragment (TRF) analysis and telomeric-FISH intensity. Mouse embryonic fibroblast (MEF) cells were harvested from different generations and genotypes of *Terc*, including G0 wild type, G0 heterozygous deletion, and G1 and G2 homozygous deletion (Fig. 1A). Considering the diversity of telomere length among tissue types, all samples' telomere were extracted from unity cell type, MEF cells. Using TRF assay (Fig. 2A) G0 wild type, with unaffected *Terc* to maintain telomere length was found to have remarkably less of shorter telomeres than both heterozygous and homozygous *Terc* deleted mice. Most G0 *Terc* heterozygous mice show slight increase of short telomeres (4000-15000 base pair). And in G1 homozygous *Terc* deletion mice, the short telomere fragments were much increase that can be observed from TRF patterns, demonstrating that complete loss of telomerase activity can directly trigger short telomere number increasing. Notably, G2 homozygous *Terc* deletion had even shorter telomeres appear, likely due to the erosion of telomeres in their parents (G1 t*Terc*) and the continued complete abrogation of telomerase function, leading to the increased number of short fragments in the TRF assay (the red labeled range: 4000 to 15000 bp), indicating telomere length decrease. In other words, these results also validate the heritability of telomerase deficiency and short telomere length.

Similar to TRF assay, no significant difference was found between G0 heterozygous *Terc* and wild type samples using telomeric-FISH staining (Fig. 3B, Appendix Fig. 2). Consistent with TRF assay, telomere intensity was greatly decreased in G2 homozygous *Terc* deletion samples (experiment conducted in quadruple) compared with wild type and G0 heterozygous. Overall, these results show a progressive increase of shorter telomere numbers in consecutive generations of t*Terc* mouse model.

2.4 Pathology of Multiple Organs

doi:10.6342/NTU202301366

2.4.1 Distortion of intestinal crypts in t*Terc* mice

In previous studies, dysfunctional telomere was found to lead to inflammation or damage in multiple organs, including disease states such as cardiomyocyte hypertrophy and fibrosis [13], idiopathic pulmonary fibrosis (IPF) [14-16] and liver cirrhosis [17, 18]. Based on the body weight decline (Fig. 2B) noted in the t*Terc* mice, their nutrient absorption part, intestine, was further investigated. Since telomerase activity is higher in stem cells, crypts – the location of intestinal stem cells (Fig. 4A), are indispensable while analyzing telomere dysfunction in the digestive system. We observed that that wild type crypts were arranged orderly and individually, while G2 t*Terc* crypts exhibited disarray and were crowed together (Fig. 4B). These phenotypes indicate atrophy or loss of crypts. Additionally, the number of crypts in the duodenum were quantified. Duodenum was chosen for analysis since it is the first part of small intestine and is important for nutrient absorption. Five duodenal areas were randomly cropped per animal and the number of crypts per 1000 μm in the cropped areas were quantified. The results showed that at 6 months old, G2 t*Terc* mice had median 12.20 crypts per mm, compare with wildtype 18.80 number/mm, there are 37.3% fewer crypts compared with the wild type mice (Fig. 4C). This decline in crypt number was more pronounced with advanced age – at 9 months, G2 t*Terc* mice had 11 crypts per mm, compared with 20.10 number/mm, showing 43.7% fewer crypts number. These results verify that telomere dysfunction induced crypts distortion in the intestine.

2.4.2 Premature structural damage in reproductive system

Infertility was noticed in telomerase deficiency animal models. Consistently, the t*Terc* mice could only be bred to the third generation (G3), accompanied by a decline in number of pups per litter with each subsequent consequent generation (Fig. 1C). To investigate

doi:10.6342/NTU202301366

the decreased litter size and infertility in later generations, testes from male animals were studied at different time points.

Under ideal conditions, the seminiferous tubule of the testis, where sperm matures, has spermatogonia located at the edge. During spermatogenesis, developing germinal cells gradually move toward the lumen. When germ cells begin to undergo the first meiotic division, they become larger in size with denser visible chromosomes, which represent cells differentiating into primary spermatocytes. During the second meiotic division, the cells return to a smaller round shape and develop into spermatids. Ultimately, as spermatozoa mature, the oval head and flagellum are formed. In addition, Sertoli cells serve as support cells between developing germinal cells and maintaining structure. A cross section of a normal mouse testis is presented in Fig. 5A.

Gross examination of wild type, G2 and G3 t*Terc* testes at 6 months showed that wild type testis was larger than G2 t*Terc* testis, and G3 t*Terc* testis was much smaller than G2 testis, showing progressively smaller testes in consecutive generations with telomerase deficiency (Fig. 5B). Histological examination of G2 t*Terc* seminiferous tubules showed severe atrophy, which may explain the reproduction obstacle (Fig. 5C). Varying levels of atrophy were observed in the seminiferous tubules of G2 t*Terc* males – from normal to severe damage. Therefore, we try to make criteria to distinguish the damage level. Damage was graded from Level 1 to Level 4 (Fig. 5D) as defined here: Level 1 – all stages of germ cells can be found, including spermatogonia, primary spermatocyte, spermatid, spermatozoa and Sertoli cells. The structure is complete and full of cells. Level 2 – mildest level of damage, with massive loss of spermatozoa. Most immature spermatocytes can still be observed. Level 3 – more serious damage with arrested spermatogenesis. Only few spermatogonia remain at the edge of the seminiferous tubule and immature spermatocytes were lost. However, the structure was maintained by

doi:10.6342/NTU202301366

Sertoli cells which were still present. Level 4 – absence of spermatogonia and germ cells of all stages. Sertoli cells remain at the boundary between connective structures and seminiferous tubule.

According to the above defined levels, the damage in wild type and G2 testes were evaluated in 6- and 9- month old male mice (Fig. 5E). At 6 months of age, level 1 (normal) tissue accounted for median 99.14% in wild type samples, showing that almost all seminiferous tubules were functional and were able to generate germ cells. However, only median 10.71% tissue was graded as level 1 (normal) in G2 t*Terc* at the same age (*p*-value<0.0001). Additionally, 21.84% in level 2, 43.38% in level 3 and 20.5% in level 4 damages were found in G2 t*Terc* testes. At 9-months of age, wild type mice showed mild aging, with level 2 damage increased to 3.11%, but large majority of seminiferous tubules (96.11%) remained fully functional at level 1. Whereas, at 9 months of age G2 t*Terc* had 24.89% level 1/normal tissue, 26.96% at level 2, 32.37% at level 3 and 15.78% at level 4 damage. Thus, telomerase deficiency affected the reproductive system in mice.

2.4.3 Pulmonary inflammation and architecture changing

Telomere attrition is associated with various diseases in multiple organs, including idiopathic pulmonary fibrosis (IPF). Given the high incidence of IPF in patients with excessive telomere erosion, the phenotype was investigated in t*Terc* model. At 6 and 9 months of age, whole lung tissue was harvested from animals and stained with hematoxylin and eosin to determine tissue damage. In total, 5 out of 13 (38.46%) six-month old G2 t*Terc* animals exhibited leukocyte infiltration, a universally recognized marker of inflammation. Similar incidence was observed in 9-month old G2 t*Terc*, with 4 out of 13 (30.77%) animals exhibiting this inflammation phenotype. In contrast, no leukocyte infiltration was observed in both age groups of wild type. Furthermore, a

doi:10.6342/NTU202301366

fibrosis-like area was observed 20% of G2 t*Terc* female lungs (Fig. 6A), suggesting remodeling of extracellular matrix components. However, no significant increase in fibrosis phenotype in 9-month old t*Terc* animals were observed. To further explore the correlation between telomeres and IPF, the senescence of type II alveolar epithelial cells (AEC II), which have been proposed to contribute to lung progenitor cells, and a known marker of IPF, was measured by staining for surfactant protein C (SPC) (Fig. 6B). The results showed a 1.4% decrease in AEC II number in G2 t*Terc* mice at 6 months, and 3.7% decrease in AEC II number at 9-months compared to wild type (Fig. 6C). These findings suggest that telomerase deficiency leads to loss of pulmonary stem cells, which might further induce the inflammation or fibrosis in lungs.

2.5 Hematology

In order to monitor physiological changes *in vivo*, the blood components of mice were recorded at three different time points – 8 weeks (sexually mature), 6 months, and 9 months, representing young and old states, respectively. Whole blood analysis was performed, measuring hematocrit (HCT), the number of red blood cells (RBC), reticulocytes (RET), white blood cells (WBC), lymphocytes (LYMPH), neutrophils (NEUT), eosinophils (EO), and monocytes (MONO).

From the blood cell component results at 8 weeks of age (Fig. 7A), it was observed that the total number of white blood cells and lymphocytes in G2 t*Terc* mice was lower than wild type mice, and this decrease can be attributed mainly due to a lower number in lymphocytes. Additionally, the RBC count in 8-week-old t*Terc* mice also showed a lower trend, particularly in females, resulting in decreased hematocrit percentage. However, compensating for the lack of RBCs, the reticulocyte number seemed to increase.

doi:10.6342/NTU202301366

At 6 months of age, the number of white blood cells in some G2 t*Terc* animals showed a tendency to recover (Fig. 7B), however, the number of lymphocytes showed a maintaining level in t*Terc* while wildtype decreased with aging; and the neutrophil also showed increasing trend at this time point. These results lead to the premature features in white blood cells. Additionally, the red blood cell count was still slightly lower than wild type, although there was no significant difference in reticulocytes.

The red blood cell counts decreased with age in both wild type and G2 t*Terc* mice, but t*Terc* mice experienced a more rapid decline in the absence of telomerase activity. Similar to the 8-week-old mice, the low number of red blood cells affected hematocrit percentage and was compensated by higher reticulocyte number. Interestingly, leukocyte count only decreased in wild type mice with age, but not in G2 t*Terc* mice. The number of leukocytes in G2 t*Terc* mice remained similar to that at 6 months, and even increased in some animals at 9 months, mainly due to a significant increase in neutrophils and monocytes. Consistently showing the early onset of aging phenotype, including lymphocyte and red blood cells decline; and also shows some inflammation features reflected on neutrophil and monocytes increasing.

These findings provide insight into the effects of telomerase deficiency on blood cell components and the potential consequences of telomere shortening on hematopoiesis in aging mice.

2.6 iG3 splenocytes analysis

Hematopoiesis arrest potentially triggered by telomerase deficiency was investigated by isolating splenic cells and staining them with immune cells markers, including B220, CD3, CD4, CD8, CD11b, CD11c, CD44, CD62L, NK1.1, F4/80, and Gr-1, which are some

doi:10.6342/NTU202301366

common inflammation markers. Consequently, the component cell types in heterozygous and homozygous *Terc* deletion iG3 mice were analyzed by flow cytometry.

Based on the flow cytometry results using markers (Table 3, Appendix Fig. 3), there were remarkable differences in leukocyte patterns between heterozygous (Fig. 8A) and homozygous (Fig. 8B) *Terc* deletion mice in iG3, including higher granulocytes, inflammatory monocytes and macrophages; and lower CD8 T cells. Specific subsets of cell populations were examined, and the lymph ocytes percentage in homozygous *Terc* deletion animals was consistently lower compared to heterozygous (Fig. 8C). Another notably change was observed in granulocytes, with a significant increase (p-value = 0.0159) in *Terc* deletion animals (Fig. 8D).

In the subtype of lymphocytes, we found out that the total number of monocytes did not differ significantly between heterozygous and homozygous animals (Appendix Fig. 4, 5), but there was an increase (p-value = 0.0327) in the inflammatory monocyte subset in *Terc* deletion animals (Fig. 8E), which suggests the systemic inflammation in these telomerase deficiency animals.

In addition, homozygous *Terc* deletion mice had lower T cells (CD3+ cells) counts in (Appendix Fig. 4, 5). Additionally, T cells were further classified into helper T cells (CD4+ cells) and cytotoxic T cells (CD8+ cells). Interestingly, CD8+ cell count was significantly decreased (p-value = 0.0159) in homozygous *Terc* deletion mice (Fig. 8F). When CD8+ T cell subtypes were analyzed, including naive T cells (Tn), central memory T cells (Tcm), and effector memory T cells (Tem) (Fig. 8G), both Tn, Tcm had a significant decline in cell frequencies in animals with complete telomerase deficiency. Consistently, CD4/CD8 ratio was increase in homozygous *Terc* deletion animals. In addition, frequency of macrophage number was increased (p-value =0.0317) in homozygous iG3 mice (Fig. 8H). On the other hand, heterozygous and homozygous *Terc*

doi:10.6342/NTU202301366

deletion mice had similar frequencies of B cells, NKT cells, NK cells, total and CD4+ T cells, total and resident monocyte (Appendix Fig. 4, 5).

In summary, these results suggest that *Terc* deletion affects leukocyte populations in a complex manner, with notable differences in granulocytes, lymphocytes, and monocyte subpopulations. These findings shed light on the importance of telomerase in hematopoiesis and the potential consequences of telomere dysfunction on immune cell development and function.

doi:10.6342/NTU202301366

Chapter 3 Discussion

In this study, we characterized shortening telomere length which is regulated by telomerase, directly triggered several phenotypes *in vivo*. Animal models with deficiency telomerase were established in the 1990s and have exhibited several pathological features from the fourth to the sixth generation [24, 25]. Here, we demonstrate that offspring with different laboratory backgrounds exhibit different processes for telomere shortening, which results in an individual timeline for the appearance of pathological features in these animals with advanced degenerative phenotypes. Furthermore, this also leads to an individual timeline of deficiency telomerase in mice [25, 27, 28]. TRF assay and telomeric-FISH results show a significant decrease in telomere length in homozygous G2 t*Terc* mice. However, it is noteworthy that the shortening of telomeres can be triggered by an existing shorter background or by an increased rate of shortening, which can be verified by precise measurement of telomere length.

Different timeline of pathological features

In most of the previous studies, the severest symptoms were presented from G4 to G6. In the small intestine, the epithelium is completely regenerated every 4 to 5 days [29], due to higher cell division. In case of telomerase impaired mice, this causes accelerated telomere erosion and DNA integrity loss, which can trigger structural damage of tissues. In previous studies, villous atrophy and zonal blunting were reported at 18-months in G6 mice [25]. Hyperplasia of the mucosa, transformation of glandular with crystalline structures, increased numbers of lymphocytes and plasma cells were observed at 12-months in G3 mice [30]. However, in this study, the pathological intestinal phenotype was advanced to 6-months in G2 mice. All of the aging phenotypes usually observed in

doi:10.6342/NTU202301366

wild type mice older than 2 years [28], were remarkably advanced in *Terc* deficiency mice, which is remarkably advanced in t*Terc* mice.

Similar to small intestinal tissue, the reproductive system is highly proliferative with germ cells possessing active telomerase in mammals to prevent rapid telomere shortening. However, in telomerase dyficiency mice, progressive mating leads to a decline in fecundity, and eventually, sterility [27]. Histological observation in previous studies showed normal structure, and fully functional reproductive system at 6 to 12 weeks age in G3 male mice [27]. However, testicular atrophy and germ cell depletion accompany infertility in G6 males, such that the generation of G7 litters is extremely rare [25, 31]. In our results, severe abnormality of testis structure and spermatocyte depletion was advanced to G2 males, with extremely rare and small litter sizes in G3.

Histological analysis of pulmonary tissues revealed that 30 – 38% of animals with telomerase deficiency displayed leukocyte infiltration phenotypes between 6- to 9-months of age, indicating tissue inflammation and injury. Interestingly, only one animal (7.6%) showed fibrosis-like phenotype in 6-months and not found in 9- months t*Terc*. These findings suggest that the shortening of telomeres may primarily influence the origin of pulmonary fibrosis. Consistently, decrease in number of AECII was observed in t*Terc* G2, which is associated with the origin of IPF[32-34]. Due to pulmonary tissue not being a highly proliferative structure compared with intestine and reproductive system, challenging pulmonary structure with cigarette [35] or bleomycin [14, 36] showed impaired tissue repair in null-telomerase mice and demonstrated lower AECII regenerative capability, which is already a hall-mark of short telomere phenotype. Hence, by extending the timeline of G2 or by using offspring of G2 t*Terc* robust fibrosis models for future studies may be established. Identifying specific cell types involved in fibrosis

doi:10.6342/NTU202301366

may be a critical aspect to define disease progress in IPF, which can be achieved using these animals.

Hematopoietic change related

With a finite lifespan, adults need to produce approximately 10^{11} – 10^{12} mature blood cells per day [37]. As highly differentiated and self-renewing cells, hematopoietic stem cells (HSCs) lose telomere length. Telomeres play a key role in hematopoietic and blood cells – as individuals age, hematological composition changes, indicating involvement of telomeres in hematopoietic aging [37-39]. We observed lower numbered total white blood cells (WBC) in young (8-week old) G2 t*Terc* mice, demonstrating that HSC differentiation was limited by lack of telomerase. Dramatic cell number decline in lymphocytes, , responsible for direct cell-mediated killing of virus-infected cells and tumor cells, and regulation of immune response, was observed in G2 t*Terc* mice [40]; granulocytes, including neutrophil, eosinophil and basophil are not only responsible for response against bacterial and others pathogen but also allergic response. The decline of these leukocytes in G2 t*Terc* indicates a defective immune system in telomerase-lacking animals.

On the other hand, several WBC types' counts, including lymphocytes, neutrophils, and monocytes, were significantly increased in 6- to 9- months aging G2 t*Terc* mice. Although WBC numbers usually decrease with age in mammals, these results revealed the opposite. As the mice were housed in an SPF environment, possibility of external infections is excluded. Therefore, we hypothesize that the increase in WBC number is triggered by organ inflammation[27]. Additionally, reticulocyte (RET) numbers were higher in both young (8-week) and aging (9-month) animals in G2 t*Terc*, indicating a disturbance in red blood cell production from bone marrow, which could be caused by

doi:10.6342/NTU202301366

anemia in telomere-deficient animals. The hematopoietic changes observed in this study may be attributed to the development of Hematopoietic stem cells (HSC), which reside in the bone marrow. It has been previously documented that bone marrow failure is caused by short telomeres [41-43]. Studies have also shown that the length of telomeres in lymphocytes and granulocytes is strongly correlated with the telomere length in Hematopoietic progenitor cells (HPC) at birth [44]. Our findings indicate that young G2 t*Terc* animals with lower RBC and WBC counts exhibit a hematological profile similar to that of aplastic anemia[43, 45], a well-known telomeric disease. Thus, the abnormal hematology observed in telomerase-deficient animals implies several potential mechanisms underlying the effects of telomere loss on hematopoiesis.

We observed an imbalance of leukocyte sub-populations in spleen of iG3 homozygous *Terc* deletion mice with a decreased frequency of lymphocytes and significantly increased frequency of granulocyte, suggesting inflammation *in vivo*. Consistently, an increase in inflammatory monocytes was found in iG3 deletion animals. Inflammatory monocytes are activated upon injury or infection and differentiate into inflammatory dendritic cells (DCs), capable of stimulating effector T cell differentiation in draining lymph nodes and inflamed tissues[46]. Consequently, lymphocytes fiercely increase in the periphery from 8-weeks to 9 months in telomerase-deficient animals. Moreover, one of the features of aging, the decline of CD8+ T cells [47], which is also one of the hallmarks of IPF [48], was evident in all iG3 mice.

Overall, the hematology results from both peripheral blood and splenocytes suggest inflammation in telomerase-deficient animals. However, a more precise examination, such as cell types in peripheral blood and cytokine profiling is still necessary.

Application of the established *Terc* $^{-/-}$ animal model for future studies

doi:10.6342/NTU202301366

Since telomere length is a reliable indicator of cellular senescence and aging, and short telomeres have been associated with an increased risk of various age-related diseases, it has strong potential for providing insight into aging and age-related diseases, such as cancer [49, 50], cardiovascular diseases, and neurodegenerative disorders.

The established animal model may help us understand the mechanisms underlying these age-related diseases and develop new interventions to treat or prevent them. From molecular aspects, telomere research provides a unique opportunity to investigate the interplay between genetic and environmental factors in the aging process, as telomere length can be influenced by both intrinsic and extrinsic factors.

Recent studies have revealed potential signaling pathways in tissues with shorter telomeres undergoing the inflammation. For example, telomere dysfunction can activate the ATM-YAP1-pro-IL-18 pathway, or uncapping of telomere can mutually reinforce the canonical Wnt signaling, furthering inflammation in intestine [51, 52]. Previous studies with regard to IPF demonstrated short telomeres activating TGF-β/Smads signaling and causing senescence of AECII in *Terc* KO mice [53, 54]. Telomere studies in animal models take long time, due to the time taken for aging and offspring generation. Due to their significantly advanced aging, t*Terc* animals are an excellent model for studying cellular aging arising as result of telomerase deficiency.

doi:10.6342/NTU202301366

Chapter 4 Materials and Methods

4.1 Animal models

For this study, C57BL/6 strain mice were acquired from National laboratory animal center, Taiwan. *Terc*$^{-/-}$ (mTR$^{-/-}$, RRID: IMSR_JAX:004132) mouse strain was acquired from The Jackson laboratory, United States. All the mice were housed and reared in the Institute of Molecular Biology, Academia Sinica. All the animal experiments in this study were performed following the IACUC approved methods by the Academia Sinica Institute of Molecular Biology's animal center.

Terc$^{-/-}$ animals from JAX were edited through targeted mutation by insertion of the neomycin resistance gene to replace the entire *Terc* gene in WW6 embryonic stem cells with C57BL/6J, 129/Sv and SJL background[24, 55], then backcrossed to C57BL/6J for at least 7 generations. *Terc*$^{-/-}$ mice are congenic to C57BL/6J expect for *Terc* gene.

4.2 Crude DNA extraction

For genotyping mice, DNA was isolated from tissue harvested from live mouse. About 0.5 cm mouse tail was cut at weaning age (after 3 wks) and digested in 400 μL NTES buffer (0.5% SDS, 50 mM EDTA, 10 mM Tris, pH-8.0) with 4 μL of 20 mg/mL Proteinase K (Merck Millipore), and incubated overnight at 60 °C with vortex frequency of 1200 rpm. After complete tissue digestion in NTES buffer, DNA was extracted using phenol/chloroform method. Briefly, 400 μL phenol/chloroform (Sigma-Aldrich, #MKCL7993) was added to the digested tissue and mixed thoroughly, and centrifuged for 10 minutes at 15,000 rpm at room temperature (RT). The separated aqueous phase was gently transferred to a new 1.5 ml micro-centrifuge tube and mixed with fresh 400 μL phenol/chloroform and centrifuged for 10 minutes at 15,000 rpm, at RT. The aqueous phase was transferred to a new tube and DNA was precipitated with 2-2.5X volume of

doi:10.6342/NTU202301366

100% ethanol, by inverting the tube until white thread-like strands of DNA become visible. The tube was centrifuged for 10 minutes at 15,000 rpm at 4 °C to spin down DNA as pellet. The supernatant was decanted completely and DNA was diluted in 50-100 μL Milli-Q water at 4°C overnight. The concentration of the extracted DNA was measured by NanoDrop® ND-1000 UV-Vis Spectrophotometer and final concentration was adjusted to approximately 200ng/mL.

4.3 Genotyping mice using PCR

To distinguish the genotype of the mice with respect to *Terc*, target regions in the DNA extracted from the heterozygous and wild type mice were amplified by PCR. To identify the mouse genotype, PCR amplicon sizes were compared. Each amplification sample contained 12.5 μL DreamTaq Green PCR Master Mix (Thermo Fisher Scientific, # K1082), 0.5 μL wild type forward primer, 0.5 μL *Terc* forward primer, 0.5 μL *Terc* reverse primer (Table 4) and 10 μL Nuclease-free water. The PCR cycling parameters are presented in Table 5. Finally, PCR products were separated through electrophoresis on 1.5% agarose gel and genotype was verified for of each sample. In the resolved PCR products, wildtype genotype product has only one band at 180 bp, heterozygous genotype has 2 bands at 180 bp and 350 bp corresponding to the wildtype and recombinant alleles, respectively, Terc deletion phenotype has one band at 350 bp corresponding to the homozygous recombinant alleles.

4.4 Mouse sacrifice

In this study, Zoletil (25mg/kg, Virbac) was utilized to sacrifice animals by over-dosing (100-150 μL) to euthanize animals by intraperitoneal injection. After 30-40 minutes, it was confirmed that the animal had stopped breathing. In addition, the animals' limbs were

doi:10.6342/NTU202301366

squeezed to verify that there was no vital sign. All the animal experiments in this study were performed following the IACUC approved methods by the Academia Sinica Institute of Molecular Biology's animal center.

4.5 Mouse embryonic fibroblast (MEF) isolation

For TRF and telomeric-FISH assay, MEF cells were isolated from pregnant female mice at 13.5 days post coitum. After shaving and sterilizing the mouse abdominal skin a cut was made with sterile scissors. The skin was pulled away to expose the abdominal wall and an incision was made. The uterine horn was lifted with forceps and the uterus was cut and transferred to a 10 cm cell culture plate containing 1X PBS (phosphate-buffered saline) on ice. The placenta and connective membranes were removed and the embryos were separated. While holding an embryo, the head above the eye was cut off and red tissue (corresponding to the heart and liver) was removed. The rest of the embryo was placed in 0.25% trypsin-EDTA and chopped into small pieces to increase trypsin efficiency. The samples were transferred into a 15 mL centrifuge tube containing 3 mL 0.25% trypsin and pipet gently several times. The samples were incubated at 4 °C for 2 hours, trypsinized at 37 °C for 10 min, and mixed gently by pipetting up and down several times, then returned to 37 °C for another 10 min. Trypsin was neutralized by adding culture medium and the isolated single cell MEFs were transferred into 10 cm cell culture plates following the conditions in Table 6.

Cells were harvested at confluence from a 15-cm culture plate. Cells (7.2×10^7) were transferred into a 15 mL centrifuge tube and centrifuged for 5 minutes at 1,000 × *g*, re-suspended with 1X PBS, and transferred to culture plate and cultured following conditions in Table 6 or frozen in 1.5 mL Eppendorf.

doi:10.6342/NTU202301366

4.6 Genomic DNA extraction.

Genomic DNA was extracted using Wizard® Genomic DNA Purification Kit (Promega #A1120). After harvesting MEF cells, 20 μg RNase A and 600 μL Nuclei lysis buffer was used to disperse the cell pellet, and incubated for 1 hour at 37°C. The lysed cell mixture was cooled to RT, 200 μL protein precipitation buffer was added, and placed at 4 °C for 15 min. Protein was precipitated by centrifuging at 4 °C, 15000 rpm for 10 min and the supernatant was transferred to a new Eppendorf tube. Then, 600 μL isopropanol was added to the supernatant and centrifuged at 4 °C, 15000 rpm for 10 min to precipitate DNA. After removing the supernatant, the DNA pellet was washed with 70% ethanol and centrifuged at 4 °C, 15000 rpm for 10 min. The supernatant was discarded and 30 – 50 μL DNA rehydration solution was added to the pellet after ethanol was completely removed. DNA was gently vortexed at 4 °C overnight and stored at 2 – 8 °C.

4.7 TRF assay

TRF (telomere restriction fragment) assay was performed to measure length of telomere. Genomic DNA was digested with Cut Smart buffer, restriction enzymes (RsaI, HinfI) and H_2O at 37°C, overnight. Pulsed-field running gel (1%) was prepared by dissolving 2 g Agarose (Bio-Rad, #1620137) in 200mL 0.5XTBE buffer using a microwave oven. The gel tank was filled and cooled till gel solidified. After solidification, samples were loaded into the gel and run following the parameters listed in Table 7.

Once the gel run was completed, the gel was dried at 50 ºC for 3 hours. The dehydrated gel was removed from the drier using R.O. water soaked filter papers. Gel was incubated in denaturation buffer (0.5 M NaOH, 1.5 M NaCl) for 20 minutes with gentle rocking, then the denaturation buffer was discarded, followed by incubation with neutralization buffer (0.5 M Tris base, 1.5M NaCl) for 20 minutes with gentle rocking.

doi:10.6342/NTU202301366

After neutralization, gel was rinsed with 4X SSC buffer. The gel was transferred to a mesh, and rolled to fit in to a glass bottle. Next, 50 mL Church buffer (0.5 M $NaPO_4$, 1 mM EDTA, 7%SDS, 1% BSA) was added to the rolled-up gel, and incubated at 50ºC for 1 hour. After discarding the used Church buffer, 500μL $(TTAGGG)_n$ labeled probe was diluted in fresh Church buffer and added to the glass tube containing the rolled gel, and incubated at 50ºC, overnight.

The buffer containing the probe was discarded the next day, and gel was washed with 4X SSC for 5 minutes, thrice, followed by washing with 4X SSC containing 0.1% SDS buffer for 5 minutes, thrice, and 2X SSC containing 0.1% SDS buffer for 5 minutes, thrice. Finally, the gel was rinsed with 4X SSC and transferred to a plastic wrap, and covered completely with it. The gel was placed on a Phosphor Imaging Plate and the plate holder was closed for 2 days. The imaging plate was scanned with Typhoon Phosphorimager (pixel: 50μm, sensitivity: 1000).

4.8 Telomeric-FISH staining

To quantify telomere length with telomeric-FISH, MEF cells isolated from embryos were cultured in a 6-cm plate for 1 week. The cells were reseeded onto coverslips within a 6-well plate and cultured for 48 hours. The coverslips were washed with 1X PBS after removing the medium, and the cells were permeabilized with CSK buffer on ice for 5 minutes. The cells were fixed with 2% paraformaldehyde (PFA) for 10 minutes at RT, and washed twice with 1X PBS. The cells were serially dehydrated by immersing the coverslips in 70%, 95%, and 100% ethanol for 5 minutes at each concentration, and air dried. The coverslips were then placed in hybridization mix[§] and denatured at 85 °C for 3 minutes. Hybridization with PNA probes was performed overnight at RT. The next day, coverslips were washed with Wash buffer I[†] & Wash buffer II[‡]. For counterstaining,

doi:10.6342/NTU202301366

DAPI was added to the second Wash buffer II and incubated for 5 minutes, and excess DAPI was washed away using Wash buffer II. The cells were serially dehydrated by immersing the coverslips in 70%, 95%, and 100% ethanol for 5 minutes at each concentration. The coverslips were mounted on slides with ProLong gold mounting medium.

§ Hybridization mix: 10 mM Tris-HCl, 70% formamide, 0.5% Blocking reagent, 5 mM telC probe

† Wash buffer I: 70% formamide, 10 mM Tris-HCl

‡ Wash buffer II: 100 mM Tris-HCl, 150 mM NaCl, and 0.08% Tween-20

4.9 Tissue harvest and preparation

Mice were euthanized with Zoletil (5 ml/kg), before harvesting organs for histological analysis.

4.9.1 Pulmonary tissue

To plump up the structure of the lung and to improve observation conditions, the blood vessels were flushed by heart perfusion. First, the ribs and diaphragm were removed from the euthanized mouse to make plenty of space for the lungs to expand. Using 27G $^{1}/_{2}$-inch needle attached to a 10 mL syringe, and 1X PBS was pumped through the left ventricle, flushed until the lungs became white. Next, an IC catheter was placed into the trachea and the lung was lavaged with 4% PFA (Sigma-Aldrich, #STBK1124) prepared by dissolving in 1X PBS (pH = 6.9).

4.9.2 Small intestine

A cut was made at the esophagus and the digestive system was completely removed from the mouse. The stomach was discarded and large intestine was excised at the cecum. In

doi:10.6342/NTU202301366

the remaining tissue, the small intestine was cut into three equal sections, the duodenum, jejunum, and ileum. A syringe was used to flush out the feces using 1X PBS, following the direction of digestion. Next, the small intestine was cut in the proximal to distal direction, and the tissue was rolled flat following the same direction.

4.10 Tissue preparation (fixation, dehydration, and wax embedding)

All the tissues were fixed in 4% PFA at 4 °C, overnight and transferred to 70% ethanol for overnight. For wax embedding, a tissue processer (Leica, TP1020) was used following the program listed in Table 8 for a total of 16 hours. The tissues embedded into paraffin blocks were stored at 4 °C at least overnight, before sections were prepared.

4.11 Histological staining

The sections were cut to 5 μm per slides by microtome. And discard front parts of block until can observed complete tissues.

4.11.1 Hematoxylin and Eosin staining

Hematoxylin and eosin stains were used in this study. The prepared tissue slides were heated in a 37 °C oven for deparaffinization, and washed with Histo-Clear (National Diagnostics, #HS200) for 10 minutes to clean the paraffin. Following this, tissue was rehydrated by immersing the slides in 95%, 90%, 70% ethanol for 3 minutes each. Staining was performed with a hematoxylin and eosin staining kit (Abcam, #ab245880). Hematoxylin staining was performed for 2 minutes, and bluing reagent was used for 1 minute for color development. Excess stain was washed away with deionized water and 100% ethanol. Next, eosin staining was performed for approximately 5 minutes, and excess was washed away with deionized water and 100% ethanol. The tissues were dehydrated by immersing slides into 70%, 95%, 100% ethanol for 3 minutes each, and

doi:10.6342/NTU202301366

cleared with xylene for 10 minutes. Finally, coverslips were mounted over the tissues with DPX mounting medium (Sigma-Aldrich, #06522).

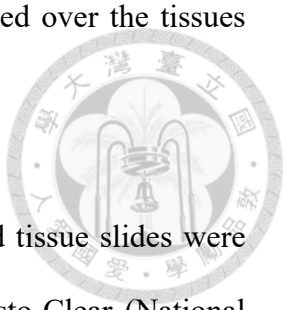

4.11.2 Immunohistochemistry staining

Hematoxylin and eosin stains were used in this study. The prepared tissue slides were heated in a 37 °C oven for deparaffinization, and washed with Histo-Clear (National Diagnostics, #HS200) for 10 minutes to clean the paraffin. Following this, tissue was rehydrated by immersing the slides in 95%, 90%, 70% ethanol for 3 minutes each. Antigen/epitope retrieval was performed by immersing the slides in boiling citrate buffer (10 mM Citric acid, 0.05% Tween, pH 6.0) in a microwave oven for 10 minutes. After cooling down the slides, the tissues were washed with 1X PBS and running water. Tissues were blocked with 1% BSA for 1 hour, and incubated with Anti-Prosurfactant Protein C antibody (Abcam, ab90716), overnight at 4 °C. The slides were washed with 1X PBS and incubated with 0.6% H_2O_2 for 10 minutes for quenching endogenous peroxidase, then washed twice with 1xPBS for 5 minutes, respectively. Next, Rabbit specific HRP/DAB (ABC) detection IHC kit (Abcam, ab64261) was used with Biotinylated Goat Anti-Polyvalent for 10 minutes, and slides were washed 3 times using 1x PBS for 5 minutes each time. Streptavidin Peroxidase was added and incubated for 10 minutes at room temperature, and washed with 1X PBS for 5 minutes, 3 times. Finally, mix DAB chromogen and DAB substrate were mixed 1:50 ratio and applied to the tissue until the color developed. Tissues were counter stained with hematoxylin and dehydrated with 70%, 95%, 100% ethanol for 3 minutes, each and cleared with xylene for 10 minutes. Finally, coverslips were mounted over the tissues with DPX mounting medium (Sigma-Aldrich, #06522).

doi:10.6342/NTU202301366

4.12 Hematopoietic analysis

Blood samples for hematologic analysis were collected through submandibular (facial) blood collection with a blood lancet at 3 weeks, 6 months, and 9 months age in a K2 EDTA tube (BD Microtainer, #365974). The samples were immediately analyzed for the percentage of blood components by ProCyte Dx (IDEXX).

4.13 Flow cytometry analysis of splenocytes

The spleen was collected from euthanized mice. The skin was opened in the abdomen, followed by ripping the peritoneum and the spleen was found on the left side of the abdomen inferior to the diaphragm. Once the spleen was removed, it was placed in cold R10 (RPMI+10%FBS), and immediately ground and filtered using a 1 ml syringe and 40 μm filter with R10. The filtrate was centrifuged for 1500 rpm at 4 °C for 5 minutes, and the supernatant was discarded. Then the pellet, which is composed of splenic cells, was treated with 10 ml RBC lysis buffer (BD biosciences, #555899) with gently pipetting and incubated for 10 minutes, next, neutralized with 40 ml R10, and centrifuged again at 1500 rpm for 5 minutes at 4 °C. The supernatant with lysis buffer, R10 and lysed red blood cells was discarded and the cells were re-suspended in 10 ml R10. Cells ($1x10^7$) were transferred into a FACS tube and centrifuged at 1500 rpm for 5 minutes at 4 °C and supernatant was discarded, and cells were washed with FACS buffer (1X PBS+ 0.5%BSA), and centrifuged again at 1500 rpm for 5 minutes at 4 °C. Cells were then incubated with 80μL FcR blocker for 15 minutes at 4 °C. Antibodies (Table 9) were added to the cells and incubated for 20 minutes at 4 °C. Next, cells were washed with FACS buffer, and centrifuged at 1500 rpm for 5 minutes at 4 °C, twice. Finally, cells were re-suspended in 1X PBS with 1% FBS on ice, stained with 2μl of 0.3 μM DAPI and analyzed using LSR II Flow Cytometer (BD biosciences).

doi:10.6342/NTU202301366

Figures

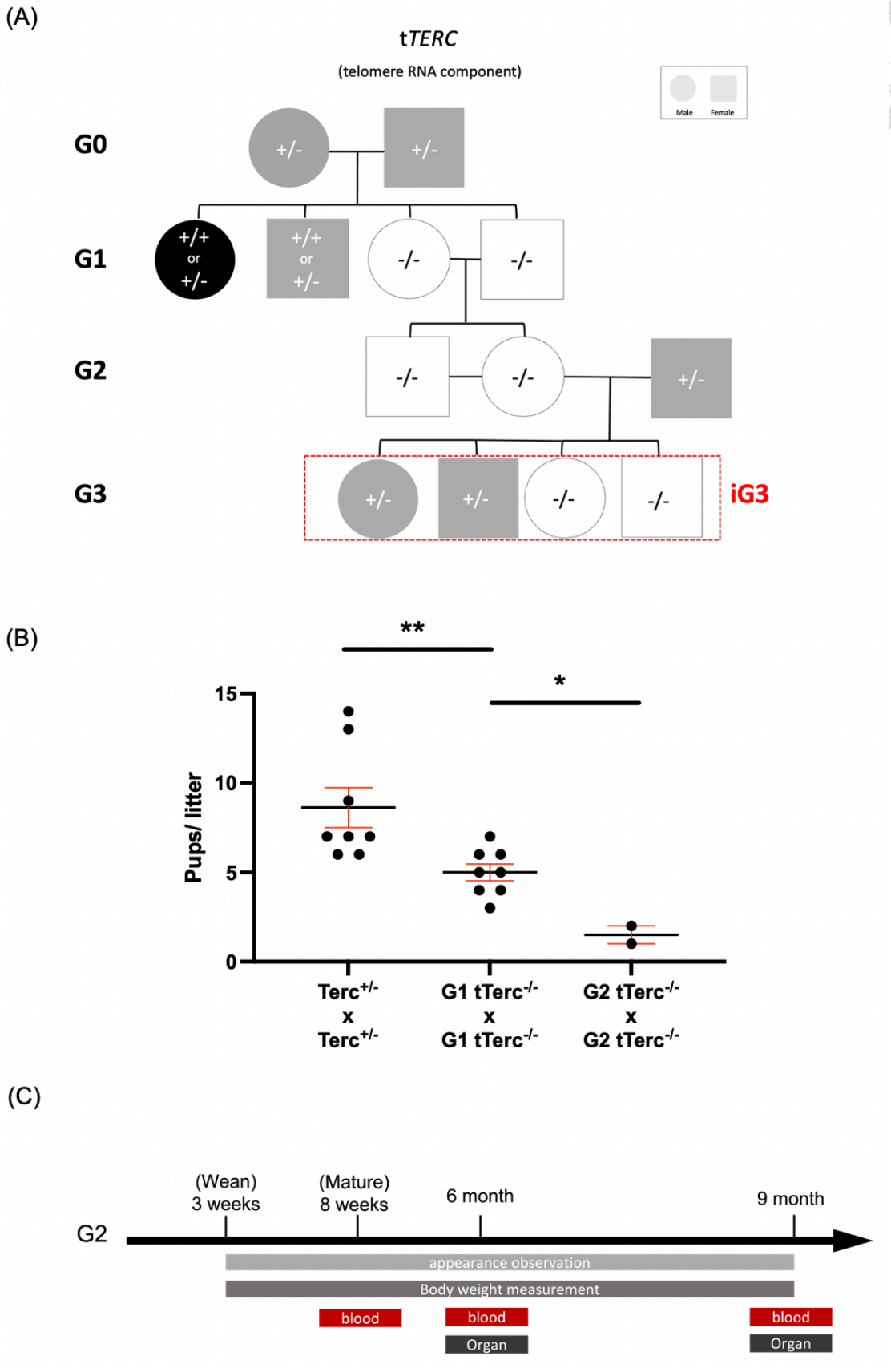

doi:10.6342/NTU202301366

Figure 1. Reproduction barrier in Terc progeny

(A) Schematic of tTerc mice progeny. Mating genotypes for Terc are shown, with wild type represented as +/+, heterozygotes as +/− and homozygotes as −/−. Dashed lines indicate reproductive impairment. iG3 was only produced by mating male homozygotes and female heterozygotes.

(B) Litter size of tTerc generations compared to wild type. Each spot represents one litter. One spot represents one litters. P values (*** $p < 0.001$; ns, non-significant) were determined by unpaired Mann-Whitney U test.

(C) Timeline of G2 pathology characterization. Body weight was recorded from 3 weeks (at weaning) till sacrifice. Blood was collected at 3 time points – 8 weeks, 6 months and 9 mon

doi:10.6342/NTU202301366

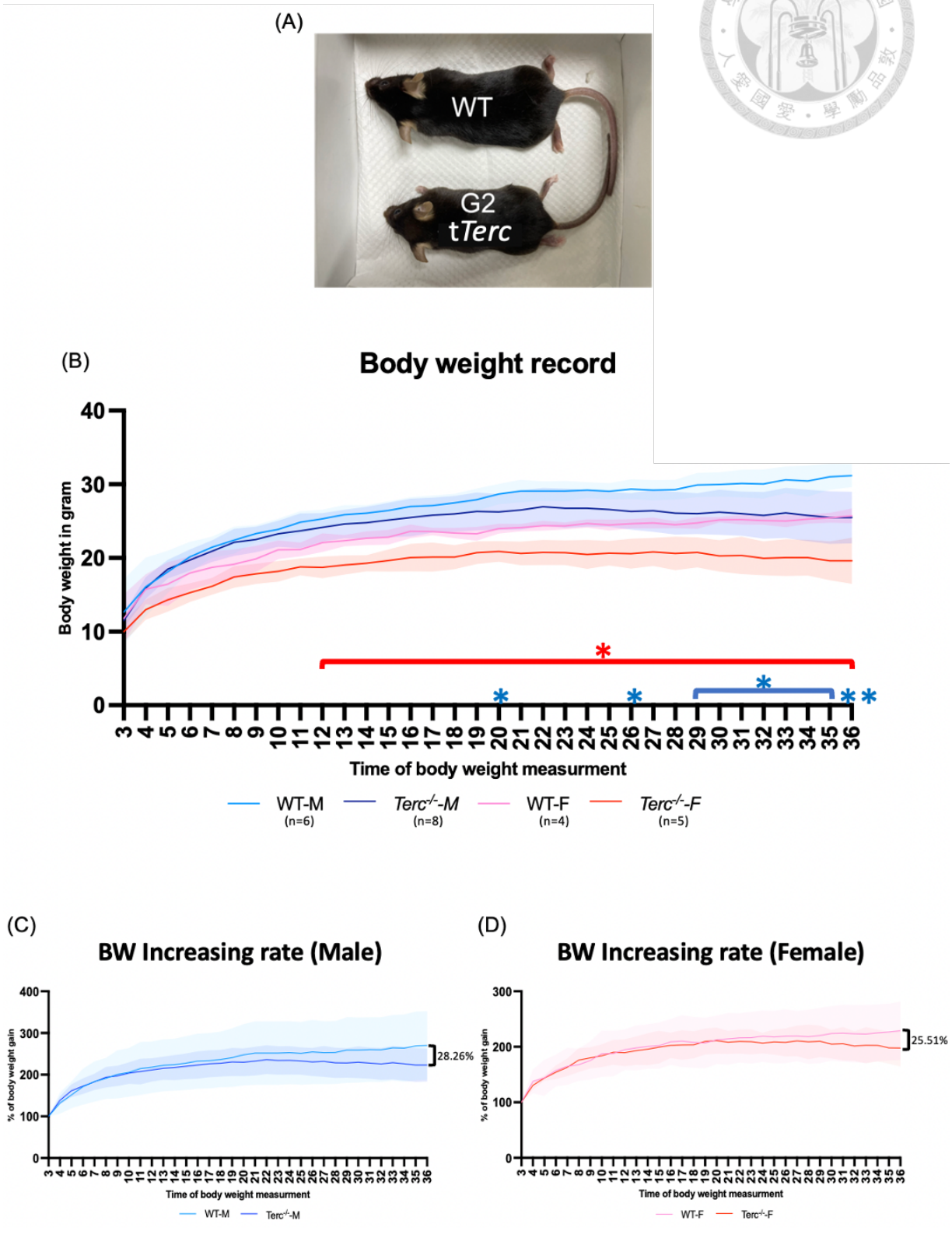

doi:10.6342/NTU202301366

Figure 2. G2 tTerc mice have smaller body size

(A) Observed difference in body size. Wild type male mouse at 6 months of age (top). Second generation (G2) tTerc male mouse at 6 months of age (bottom).

(B) Body weight record. Body weight was recorded from weaning age (3 weeks) to sacrifice (36 weeks). (Wild type male, n=6; wild type female, n=4; G2 tTerc male, n=8; G2 tTerc female, n=5)

(C, D) Rate of weight gain. The percentage of body weight gain was calculated by dividing body weight at each week to weight at weaning. The rate of body weight gain in male (C) and female (D) mice are shown.

doi:10.6342/NTU202301366

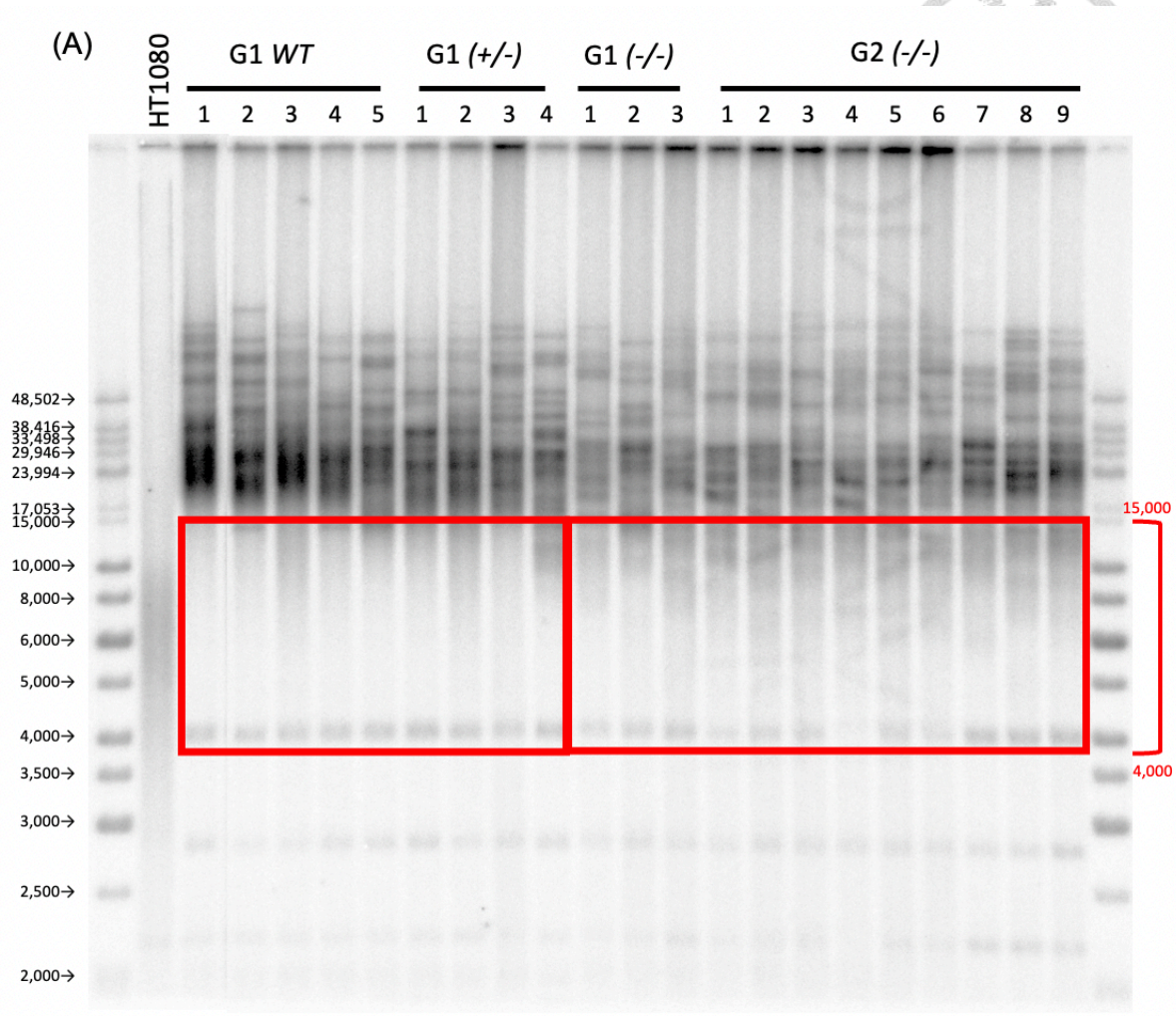

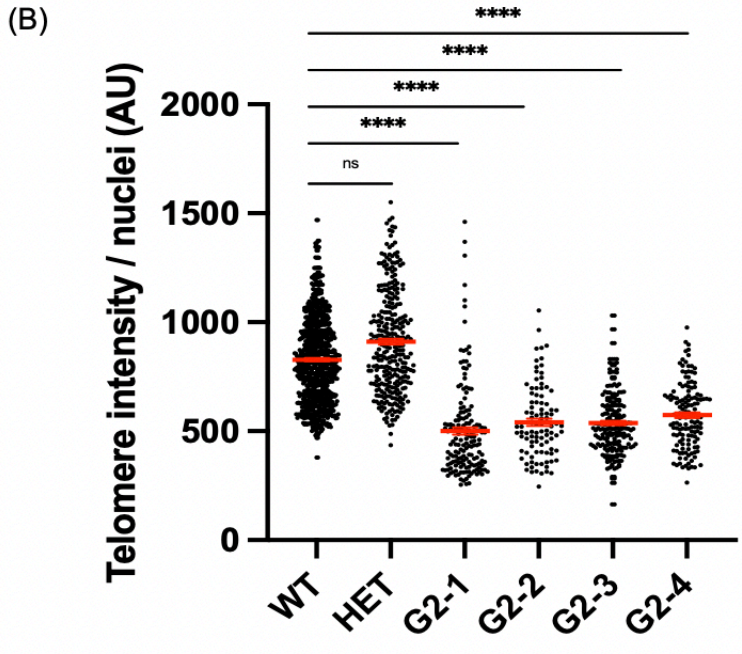

doi:10.6342/NTU202301366

Figure 3. Shorter telomeres in progeny tTerc generation

(A) Telomere length in tTerc mice. TRF assay was used to visualize telomere length distribution in mice with different grades of telomerase deficiency and of different generations. Genomic DNA samples for TRF assay were extracted from MEF, isolated from embryos at 13.5 days post-coitum and cultured for 1 week. Red box showing the 4000 to 15000 bp size of fragment telomere.

(B) Telomere length quantification by telomeric-FISH. Telomere length was measured by measuring the intensity of fluorescence conjugated with telomeric sequence probes. MEFs from different embryos, including wild type (n=1, 431 MEF cells counted), heterozygous (n=1, 325 MEF cells counted), G2 homozygous-1 (n=1, 165 MEF cells counted), G2 homozygous-2 (n=1, 96 MEF cells counted), G2 homozygous-3 (n=1, 109 MEF cells counted) and G2 homozygous-4 (n=1, 142 MEF cells counted) were analyzed. Cells were cultured for 1 week after isolation from embryo and fixed on a coverslip, and hybridized with telomeric sequence probes. Images were analyzed using FIJI image processing package. Each dot represents one cell. P values (**** $p < 0.001$; ns, non-significant) were determined by unpaired Mann-Whitney U test.

doi:10.6342/NTU202301366

(A)

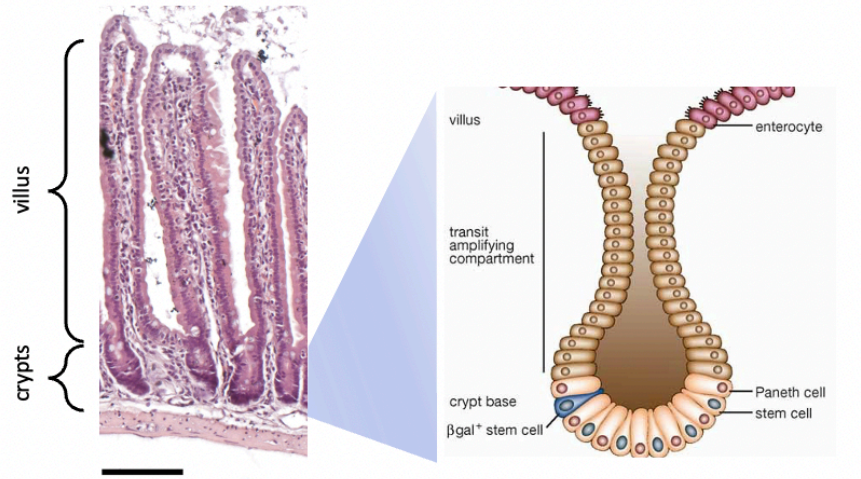

(Clevers, H. 2009)

(B)

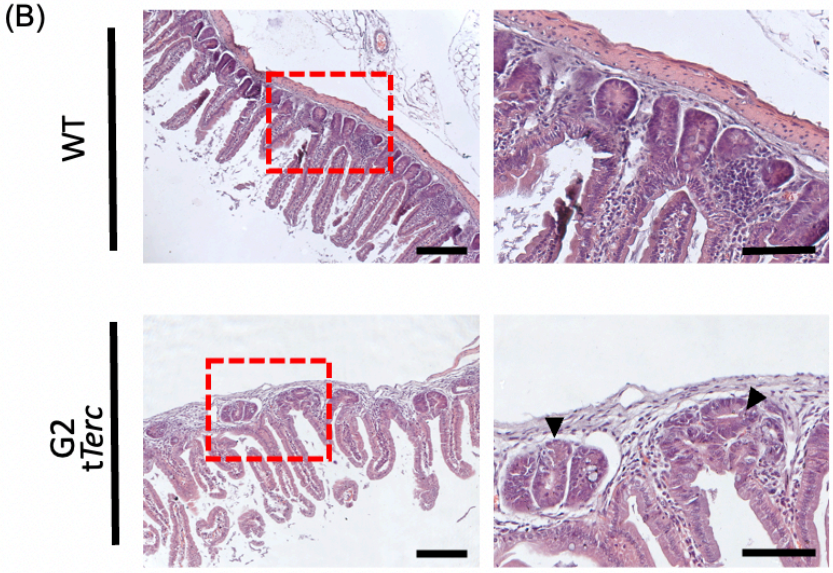

(C)

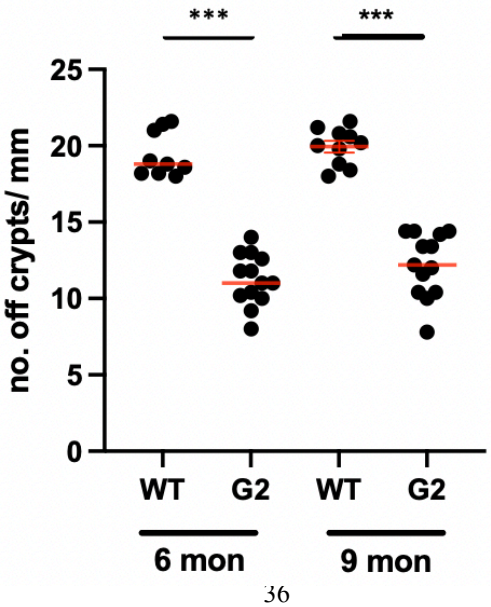

doi:10.6342/NTU202301366

Figure 4. Intestinal crypts distortion in G2 tTerc mice

(A) Crypt structure. (Left) Location of crypts in duodenum containing villus and crypts in histological samples stained with H&E (scale bar = 100 μm). (Right) Diagram of intestinal crypts[56].

(B) Crypt phenotype in G2 tTerc and wild type. Histology of duodenum of male wild type and G2 tTerc at 6-months, stained by H&E, showing whole structure (scale bar = 100 μm). Inset: Enlarged image emphasizing crypt structure (Scale bar = 50 μm). Arrows show the distortion of crypts.

(C) Quantification of crypt number. Number of crypts in 1000 μm from randomly selected duodenal segments were quantified, and the process was repeated in 5 different areas in each animal. One spot represents one animal. P values (*** $p < 0.001$; ns, non-significant) were determined by unpaired Mann-Whitney U test.

doi:10.6342/NTU202301366

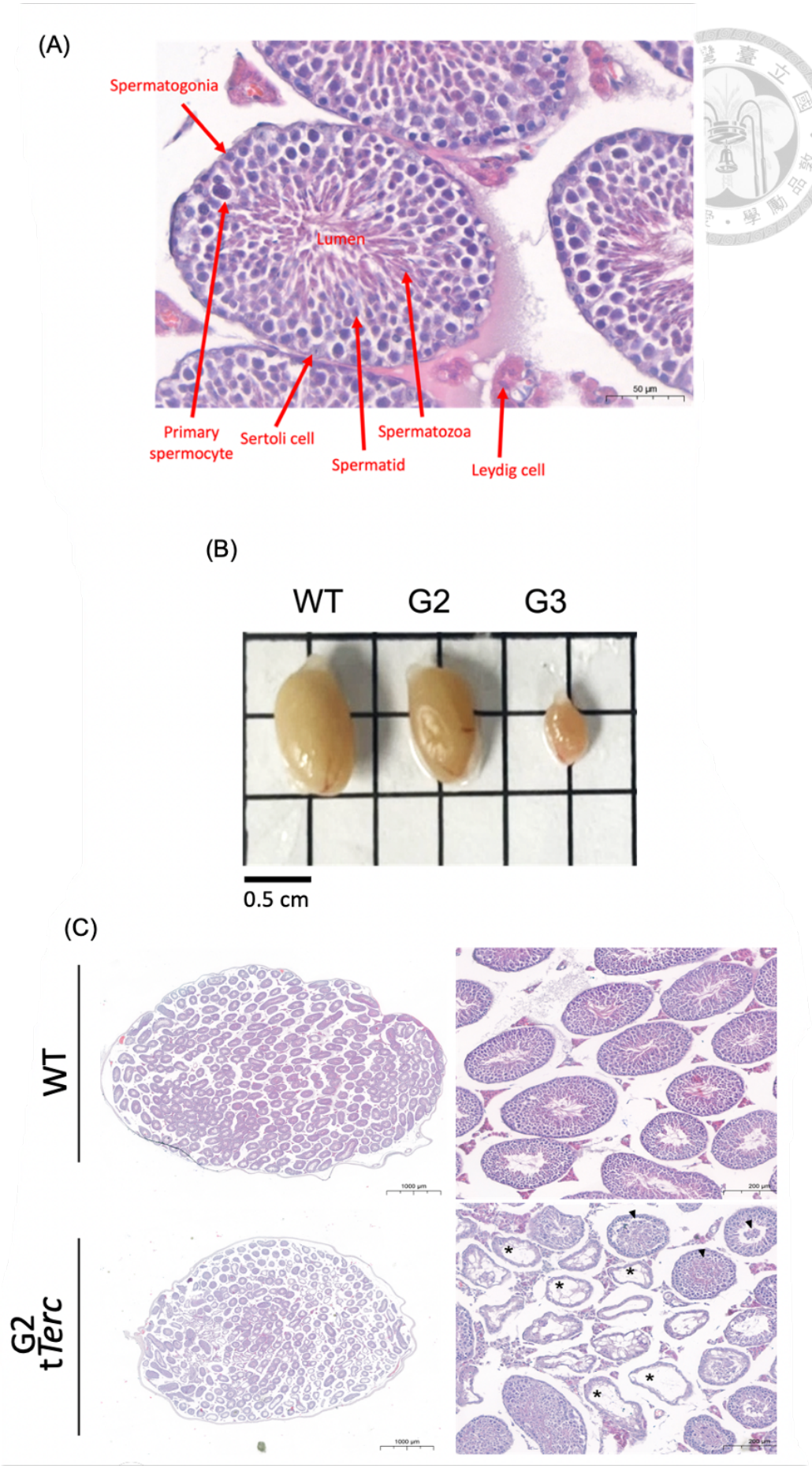

doi:10.6342/NTU202301366

(D)

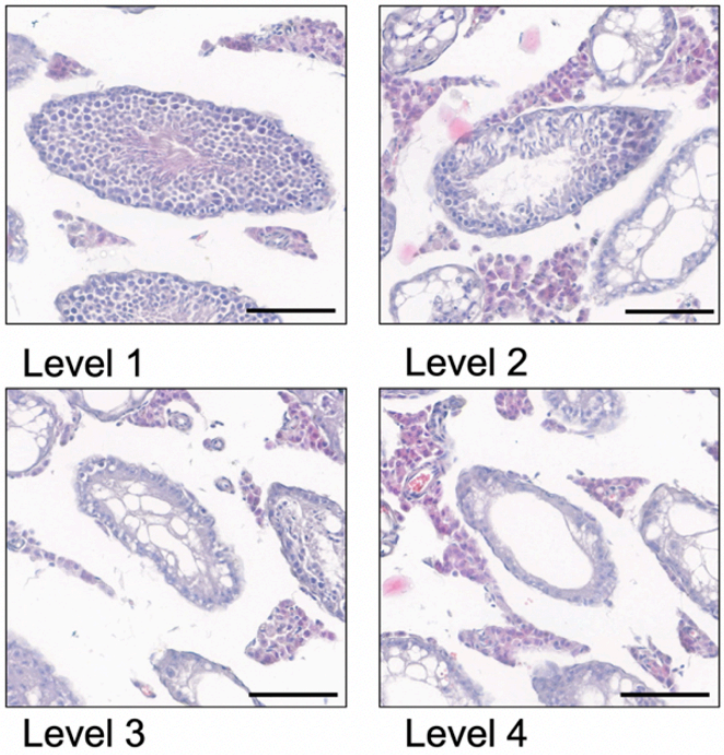

(E)

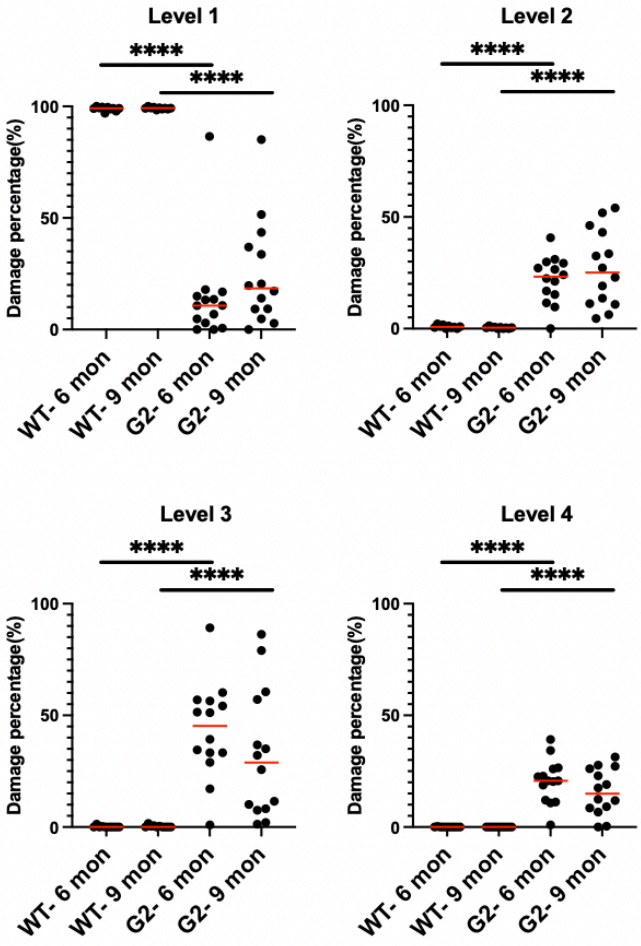

doi:10.6342/NTU202301366

Figure 5. Premature degeneration of testicle in G2 t*Terc* mice

(A) Normal testicle structure. H&E staining of 6-months old wild type testis showing seminiferous tubules, the environment of spermatogenesis. During spermatogenesis spermatogonical stem cells gradually move from the edges to the center, and ultimately mature spermatozoa leave through the lumen.

(B) Gross examination of testis. At 6 months of age, G2 t*Terc* mice testis was slightly smaller than wild type, and G3 t*Terc* testis was dramatically smaller than G2 testis.

(C) Testicle phenotype in G2 t*Terc* mice. Testicular morphology in 6- month old wild type (top) and G2 t*Terc* (bottom) observed after H&E staining. Sloughed germ cells (arrow), and debris tubule (asterisks) are shown in G2 t*Terc*.

(D) Damage level in testis. Four levels of damage were defined by the loss of immature spermatic cells and structural collapse after H&E staining was performed (scale bar = 50 μm).

(E) Percentage of testicle damage. Testicular damage was quantified **(D)** at 6-months and 9-months of age. (Wild type at 6 months, n=6; G2 t*Terc* at 6 months, n=8; wild type at 9 months, n=6; G2 t*Terc* at 9 months, n=8). One spot represents one testis. P values (**** $p < 0.0001$) were determined by unpaired Mann-Whitney U test.

doi:10.6342/NTU202301366

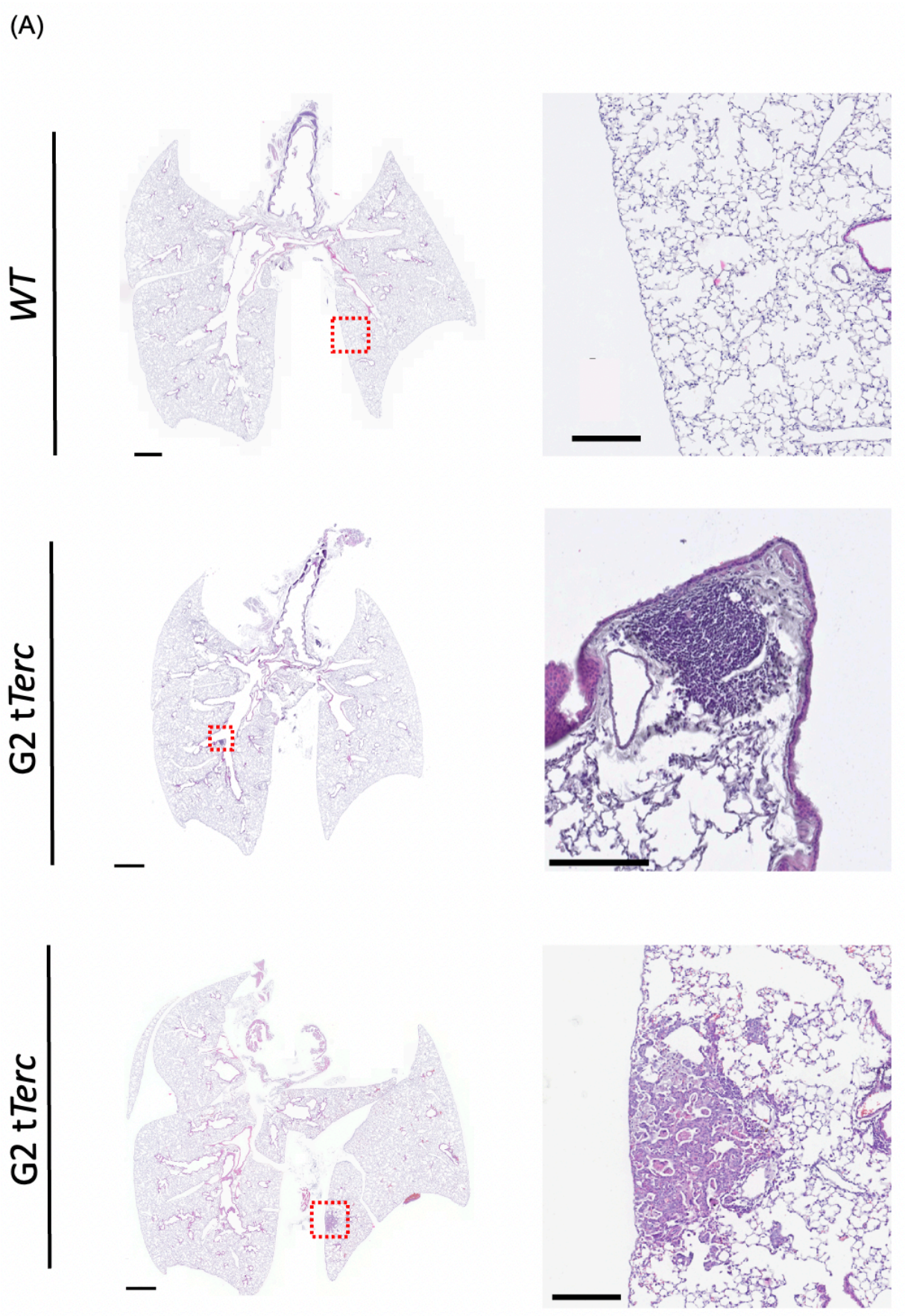

doi:10.6342/NTU202301366

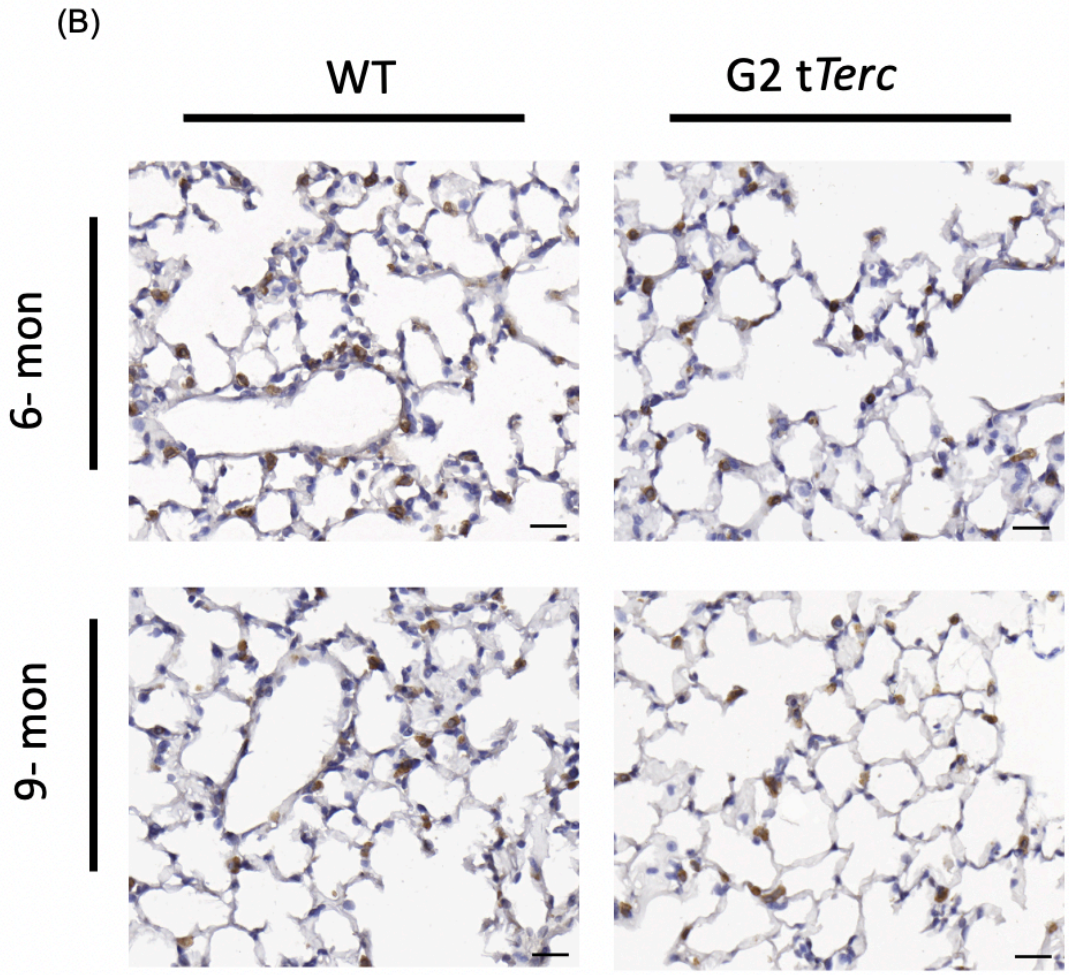

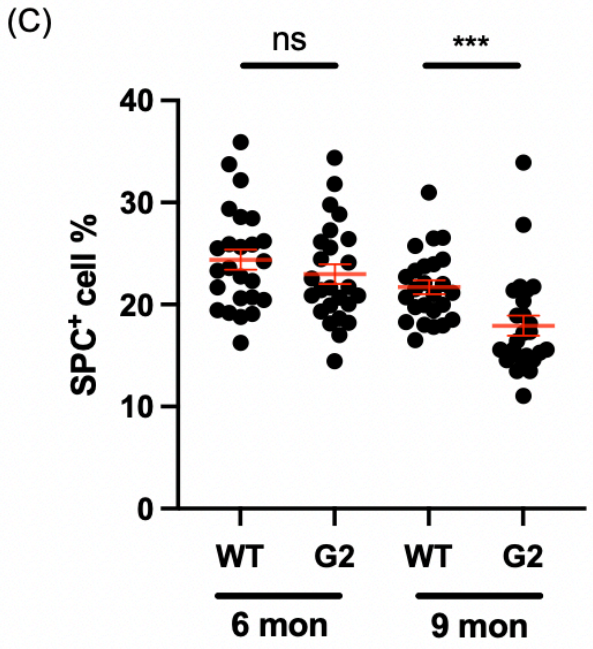

doi:10.6342/NTU202301366

Figure 6. Pulmonary abnormality in G2 t*Terc* mice

(A) Pulmonary phenotype in G2 t*Terc* mice. Lung tissue of 6-month old mice stained with H&E – wild type (Top) and G2 male (Middle) with leukocytes infiltration phenotype, and G2 female (Bottom) with fibrosis-like area. Left panel shows whole lung tissue (scale bar = 1000 μm), and right panel shows the magnified inset (scale bar = 200 μm).
(B) Immunohistochemistry of AEC II. Staining with SPC antibody, a marker of AEC II to measure senescence of self-renewing cells (Scale bar = 20 μm).
(C) Quantification of AEC II percentage. Percentage of SPC^+ cells was calculated after staining. Analysis of images was performed using FIJI and Labkit image processing packages. Unpaired Mann-Whitney U test p-values indicate statistical significance, (*** $P < 0.001$; ns, non-significant).

doi:10.6342/NTU202301366

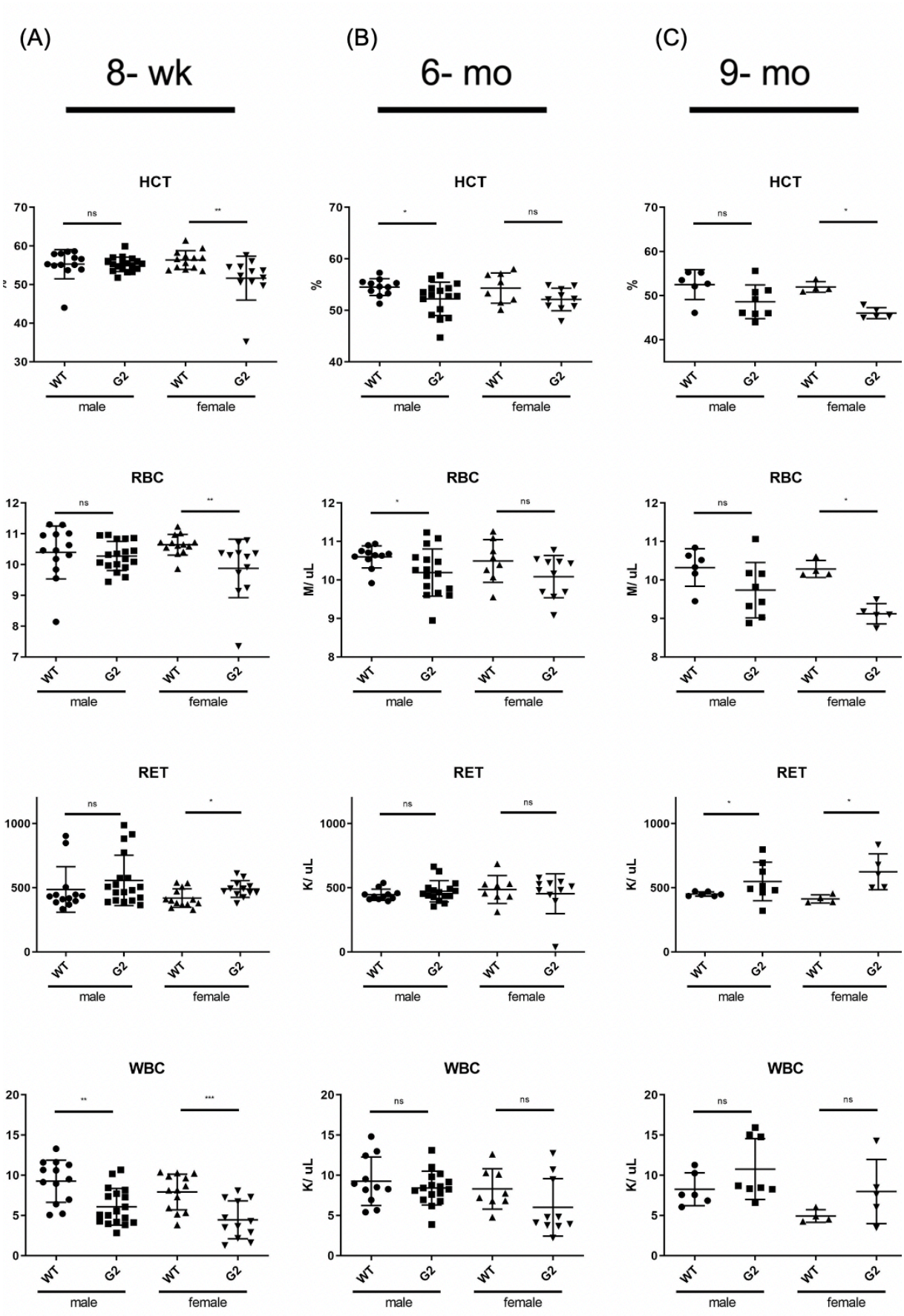

doi:10.6342/NTU202301366

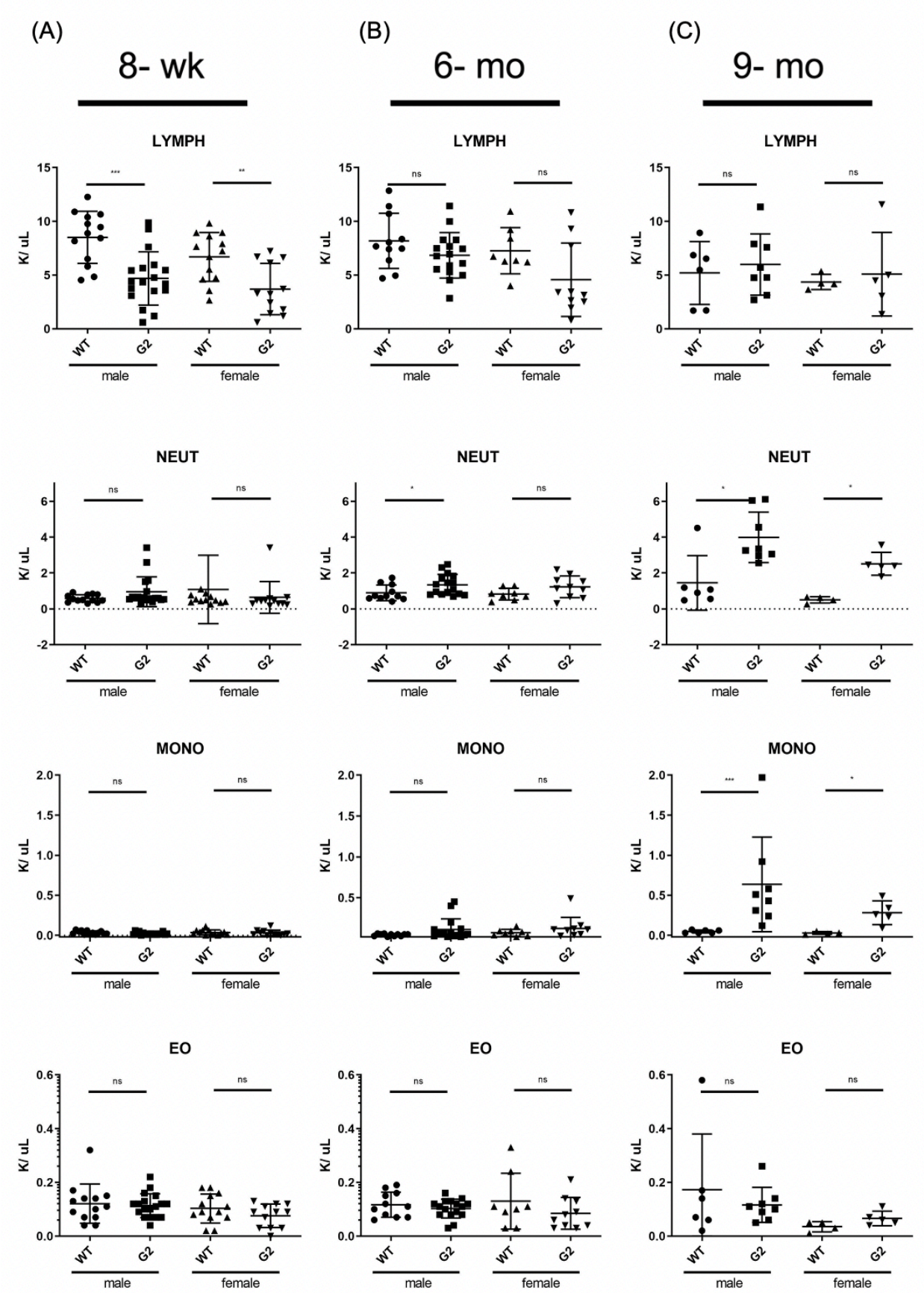

doi:10.6342/NTU202301366

Figure 7. Change in whole blood composition in G2 t*Terc* mice at different time points

(A, B, C) Mouse peripheral blood was collected from the submandibular vein at 8 weeks (A), 6 months (B) and 9 months (C). All blood samples were analyzed by ProCyte DX (IDEXX). Unpaired Mann-Whitney U test was used to determine statistical significance, between mice genotypes (* $P < 0.05$; ** $P < 0.01$; ns, non-significant).

doi:10.6342/NTU202301366

(A)

iG3*(+/-)*

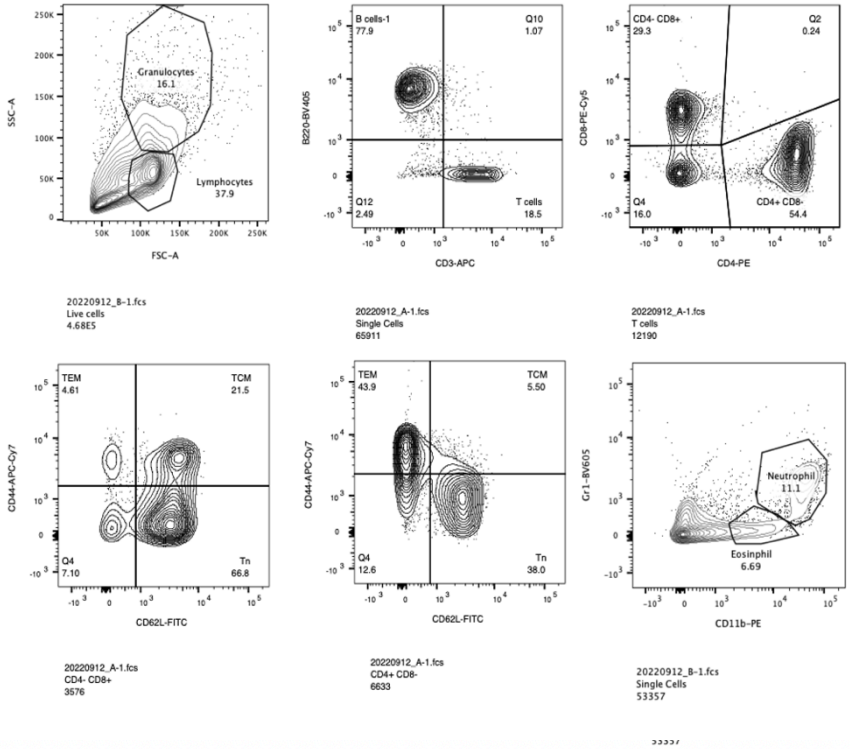

(B)

iG3*(-/-)*

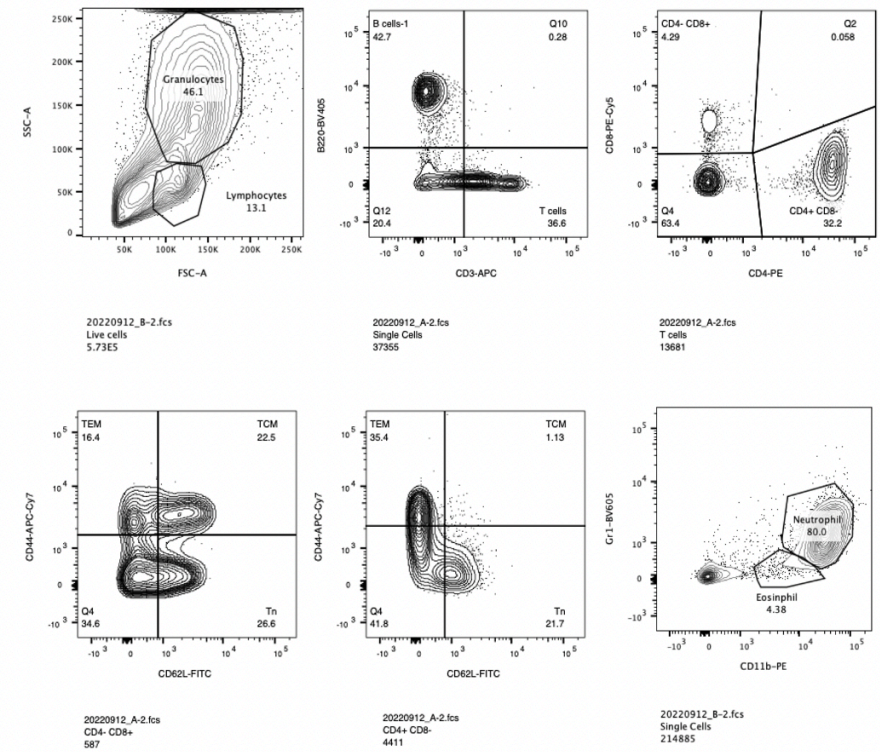

doi:10.6342/NTU202301366

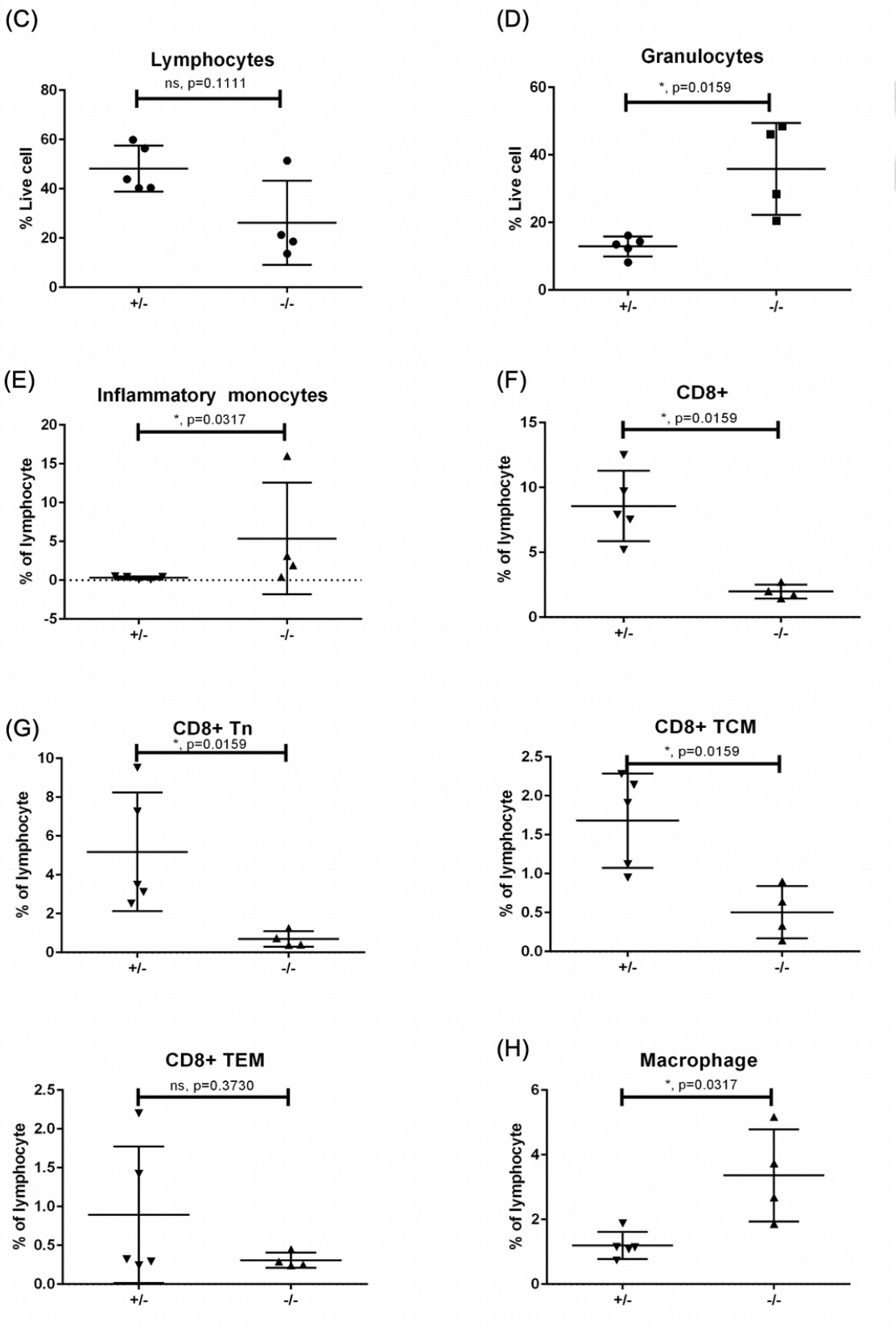

doi:10.6342/NTU202301366

Figure 8. Comparison of splenocyte composition in *Terc* heterozygous and homozygous deletion iG3 mice

(A, B) Representative **flow cytometry results of iG3 splenocytes.** Splenocytes from 9-month old iG3 heterozygous **(A)** and homozygous *Terc* deletion **(B)** mice were characterized using FACS analysis as lymphocytes, including B cells and T-cell subsets (CD4 and CD8 subtypes), NK cells, NKT cells, monocytes (inflammatory and resident monocytes), and granulocytes including neutrophils and eosinophils.

(C, D) Frequencies of lymphocytes, granulocytes numbers in iG3. Granulocytes were gated as Gr-1^{high} and $CD11b^{high}$, with total live cells as 100%. Samples analyzed - Heterozygous, n=5 and Homozygous, n=4. Mann-Whitney U unpaired test student p-values indicate statistical significance, *P* values (* $P < 0.05$; ns, non-significant).

(E-G) Inflammatory monocyte and CD8+ T cell numbers in iG3. Inflammatory monocytes were gated as CD11b+, CD11c+ and Gr-1^{mid}. T-cell subsets were gated for the $CD8^{+}$ and $CD4^{-}$ from cells expressing CD3**.** CD8+ cells were further classified into central memory ($CD44^{high}$ and $CD62L^{high}$), effector memory ($CD44^{high}$ and $CD62L^{low}$) and naïve ($CD44^{low}$ and $CD62L^{high}$) T cells, with Lymphocytes cell number as 100%. Samples analyzed - Heterozygous, n=5 and Homozygous, n=4. Mann-Whitney U unpaired test student p-values indicate statistical significance, *P* values (* $P < 0.05$; ns, non-significant).

(H) Macrophage numbers in iG3. Macrophages were gated as F4/80+, with Lymphocytes cell number as 100%. Samples analyzed - Heterozygous, n=5 and Homozygous, n=4. Mann-Whitney U unpaired test student p-values indicate statistical significance, (* $P < 0.05$; ns, non-significant).

doi:10.6342/NTU202301366

Appendix

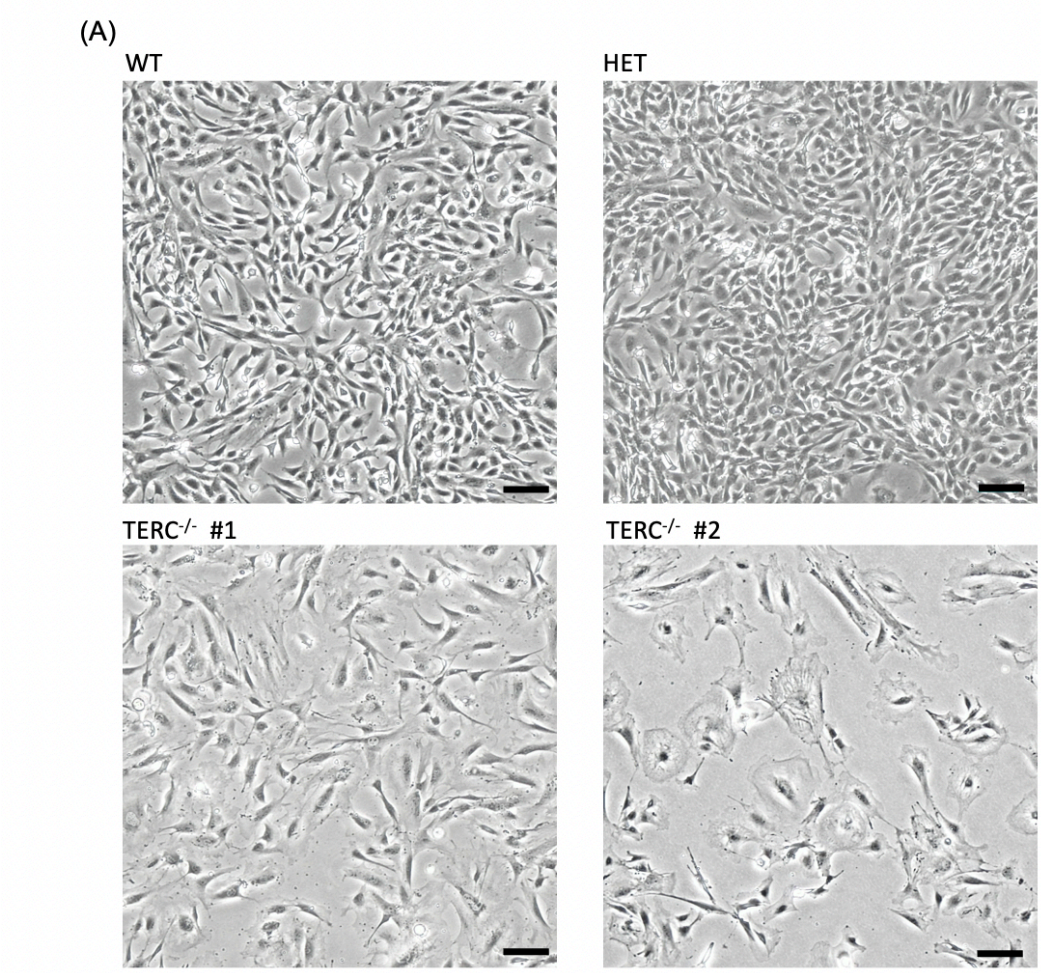

Appendix Figure 1. Lower growth rate of telomerase deficiency cells

(A) G2 Mouse embryonic fibroblast cell growth in culture. Representative images of MEF cells isolated from wild type (WT), G0 heterozygous *Terc* deletion (HET) and 2 independent G2 homozygous *Terc* deletion (*Terc*$^{-/-}$#1, *Terc*$^{-/-}$#2) embryos cultured for 7 days in DMEM supplemented with 10% FBS, maintained at 5% CO_2, 3% O_2 at 37 °C. (scale bar = 100 μm)

doi:10.6342/NTU202301366

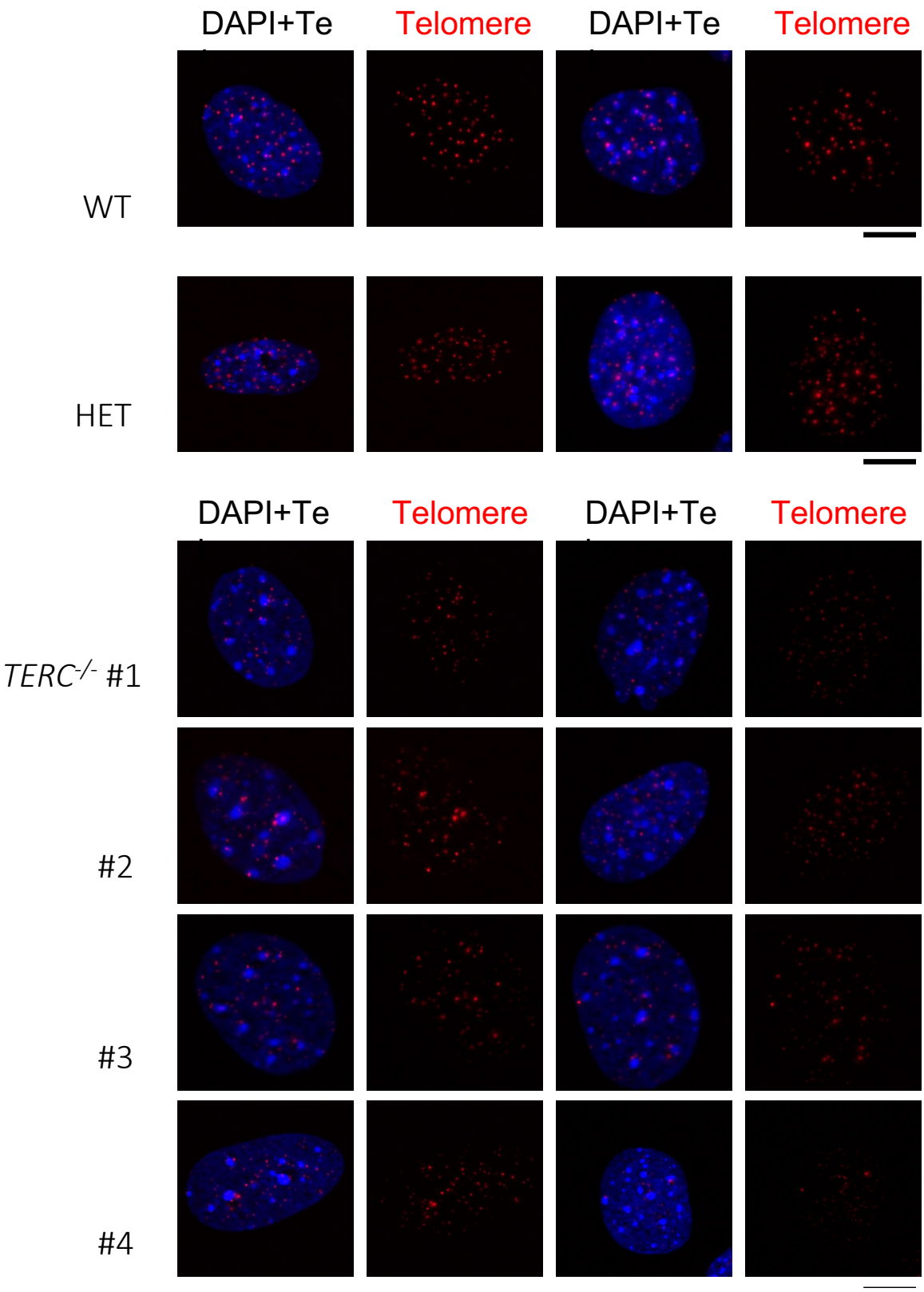

doi:10.6342/NTU202301366

Appendix Figure 2. Shorter telomere in G2 t*Terc* cells

(A) Telomeric-FISH staining. Representative images of MEF cells isolated from wild type (WT), G0 heterozygous *Terc* deletion (HET) and homozygous *Terc* deletion ($Terc^{-/-}$ #1, #2, #3, #4 indicate 4 $Terc^{-/-}$ mice). MEF was cultured for 7 days in DMEM with 10% FBS, maintained at 5% CO_2, 3% O_2 at 37 °C (scale bar = 100 μm). Cells were stained using telomeric primer (red) and DAPI (blue) and images were obtained using a deconvolution microscope.

doi:10.6342/NTU202301366

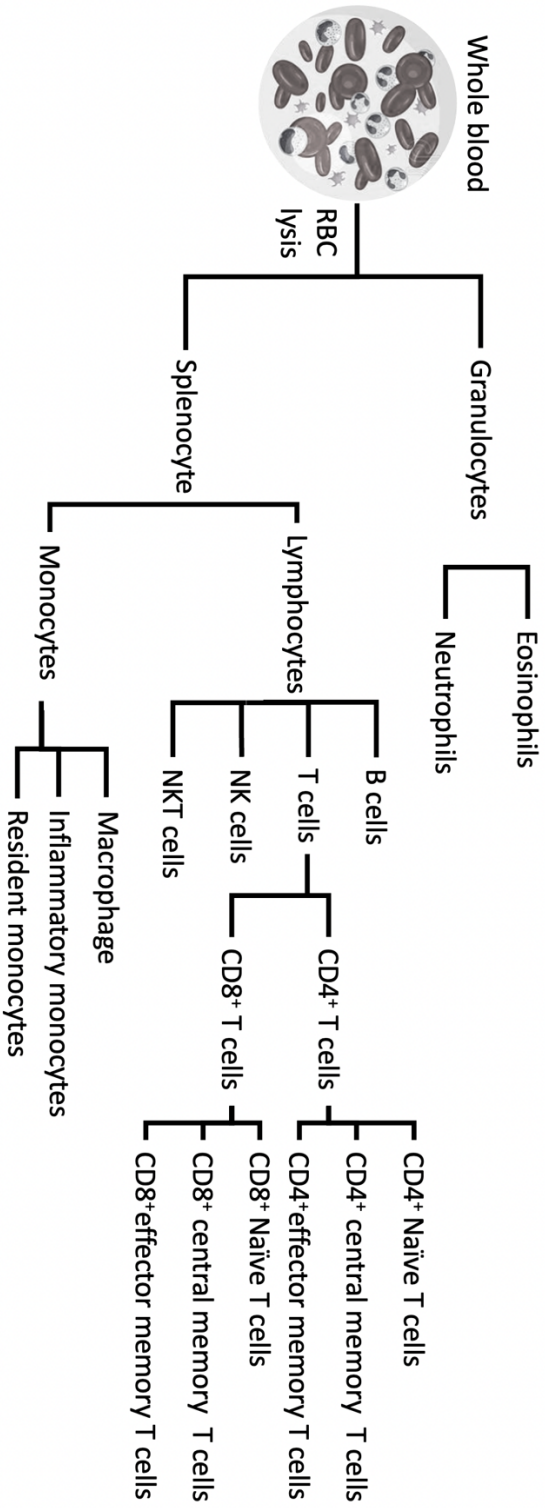

Appendix Figure 3. Cytometry gating strategy

(A) Gating strategy. Utilized iG3 splenic cells and lysis red blood cells. Gating by specific marker to separate different types of blood cells.

doi:10.6342/NTU202301366

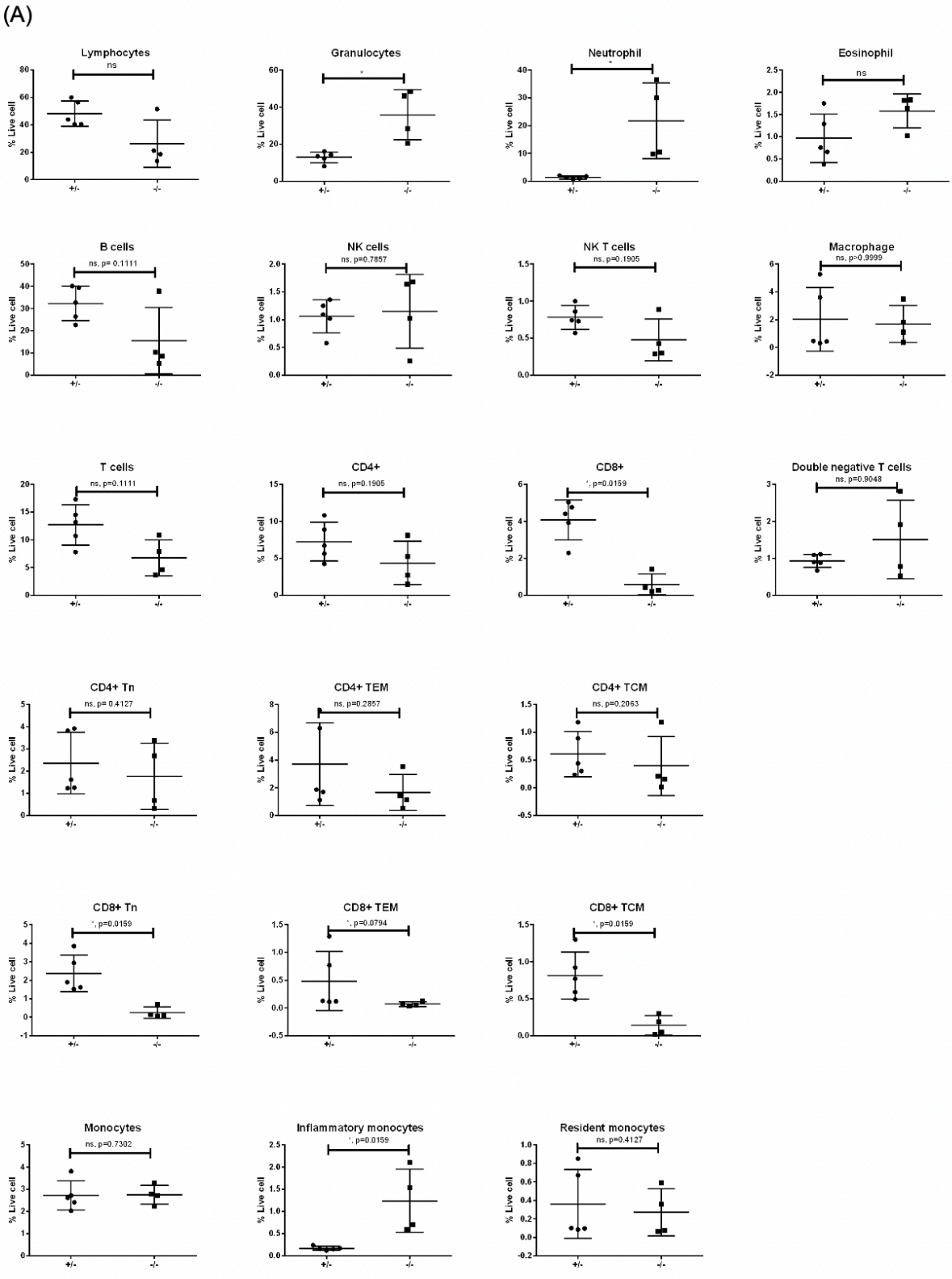

Appendix Figure 4. Blood cell composition changed in iG3 splenocyte

(A) Flow cytometry results of iG3 splenocytes. Splenic cell components from 9-month old iG3 heterozygous and homozygous *Terc* deletion mice were analyzed using flow

doi:10.6342/NTU202301366

cytometry, with total live cells as denominator. Mann-Whitney U unpaired test student p-values indicate statistical significance. (* $P < 0.05$; ns, non-significant).

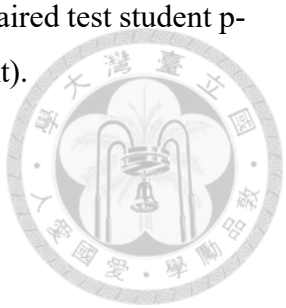

doi:10.6342/NTU202301366

(A)

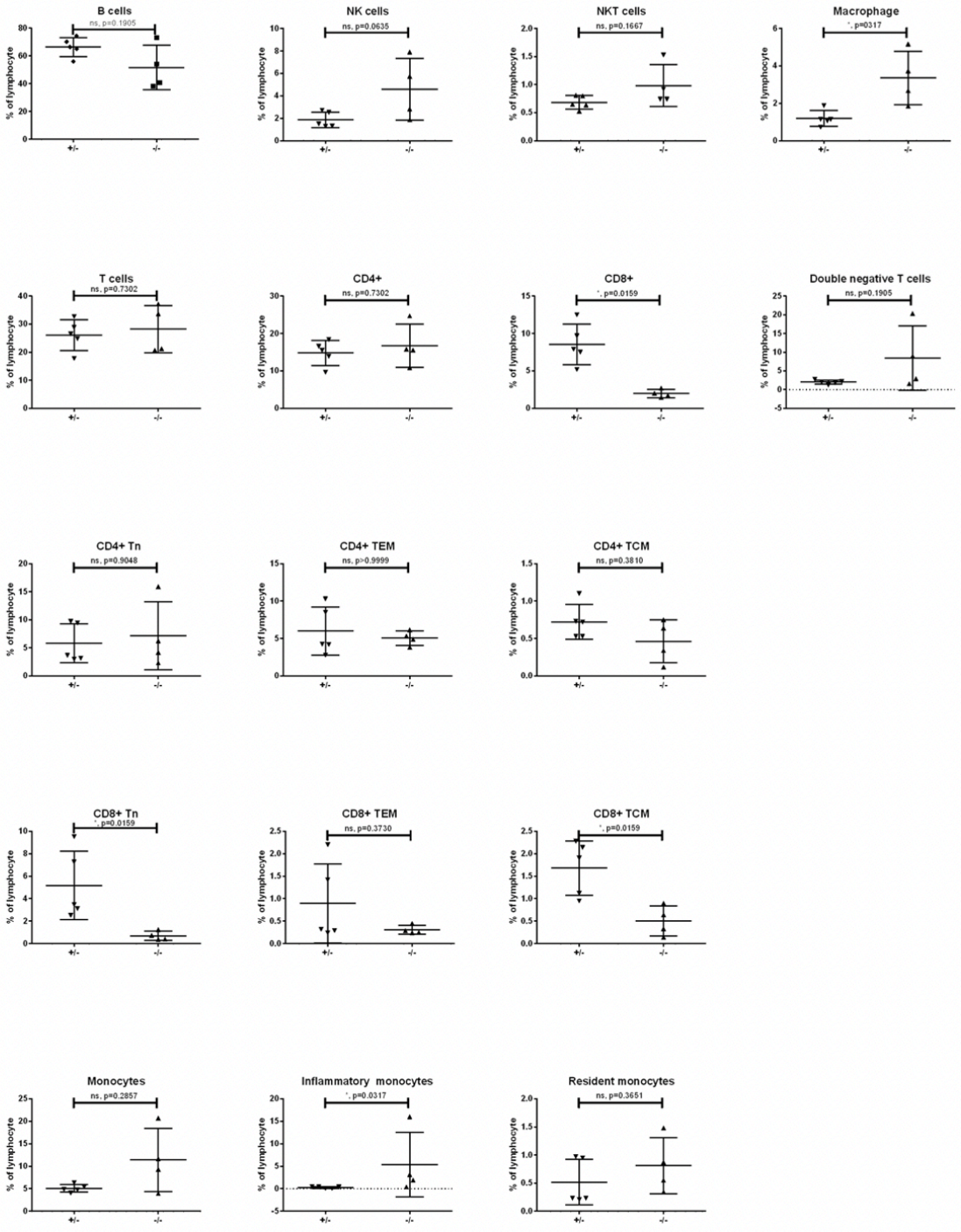

doi:10.6342/NTU202301366

Appendix Figure 5. Lymphocytes composition changed in iG3 splenocyte

(A) Flow cytometry results of iG3 splenocytes. Splenic cell components from 9-month old iG3 heterozygous and homozygous *Terc* deletion mice were analyzed using flow cytometry, with total lymphocytes as denominator. Mann-Whitney U unpaired test student p-values indicate statistical significance, (* $P < 0.05$; ns, non-significant).

doi:10.6342/NTU202301366

Tables

Table 1. Average body weight at 4 different time points

Genotype-Sex / Age at measurement	WT-M	WT-F	Terc-M	Terc-F
8 wk	22.405	19.135	22.132	17.420
4 mon	26.986	23.612	25.486	20.058
6 mon	29.205	24.677	26.755	20.490
9 mon	31.198	25.705	25.490	19.600

Average body weight is presented in grams

Table 2. Body weight increasing rate at 4 different time points

Genotype-Sex / Age at measurement	WT-M	WT-F	Terc-M	Terc-F
8 wk	176.904	192.372	162.332	174.234
4 mon	213.080	221.523	200.318	200.620
6 mon	230.596	232.551	209.353	204.940
9 mon	246.335	221.555	218.069	196.039

Body weight increase is presented in percentage

Table 3. Sorted-marker in FACS analysis

Cell type	Marker
Granulocyte	$DAPI^-$, $CD11b^+$, $Gr\text{-}1^{high}$, SSC^{high}
Eosinophil	$DAPI^-$, $CD11b^+$, $Gr\text{-}1^{low}$, SSC^{high}
Monocyte	$DAPI^-$, $CD11b^+$, SSC^{low}
Inflammatory Monocyte	$DAPI^-$, $CD11b^+$, $CD11c^-$, $Gr\text{-}1^{mid}$
Resident monocyte	$DAPI^-$, $CD11b^+$, $CD11c^+$, $Gr\text{-}1^-$
B cell	$DAPI^-$, $B220^+$
NK cell	$DAPI^-$, $CD3^-$, $NK1.1^+$
Macrophage	$DAPI^-$, $F4/80^+$

doi:10.6342/NTU202301366

T cell	DAPI^{-}, CD3^{+}
NK T cell	DAPI^{-}, CD3^{+}, NK1.1^{+}
CD4^{+} T cell	DAPI^{-}, CD3^{+}, CD4^{+}
CD8^{+} T cell	DAPI^{-}, CD3^{+}, CD8^{+}
Effector memory T cell (T_{EM})	DAPI^{-}, CD3+, CD44^{high}, CD62L^{low}
Central memory T cell (T_{CM})	DAPI^{-}, CD3+, CD44^{high}, CD62L^{high}
Naïve T cell (Tn)	DAPI^{-}, CD3+, CD44^{low}, CD62L^{high}

Table 4. Primer sequence for PCR

Primer	Sequence
Wildtype (Forward)	5'- GCA CTC CTT ACA AGG GAC GA -3'
t*Terc* (Forward)	5'- ATT TGT CAC GTC CTG CAC GAC G -3'
Wildtype & t*Terc* (Reverse)	5'- CTT CAA TTT CCT TGG CTT CG -3'

Table 5. Terc PCR cycling parameter

Steps	Temperature	Time
Initial Denaturation	95 °C	3 min
36 cycles	95 °C	30 sec
	60 °C	30 sec
	72 °C	1 min
Final extension	72 °C	1 min
Hold	4 °C	

Table 6. MEF cell culture condition

Cell name	Organism	Cell type	Culture medium	Culture conditions

doi:10.6342/NTU202301366

MEF	Mus musculus	Fibroblast	DMEM + 10% FBS + 0.1 mM β-mercaptoethanol	37 °C, 3% O_2, 5% CO_2

Table 7. Parameters for resolving digested gDNA on pulsed field gel in TRF

Temperature	14˚C
Electricity	5 volt/cm
Run Time	16.5 hrs
Initial switch time	0.5 sec
Final switch time	6 sec
Water Flow speed	700 ml/min

Table 8. Program used for embedding tissues in wax

Solution	Time
70% ethanol	1 hr 15 min
80% ethanol	1 hr 15 min
90% ethanol	1 hr 15 min
95% ethanol (1)	1 hr 15 min
95% ethanol (2)	1 hr 30 min
100% ethanol (1)	1 hr 15 min
100% ethanol (2)	1 hr 15 min
100% ethanol (3)	1 hr 30 min
Xylene (1)	1 hr 15 min
Xylene (2)	1 hr 30 min
Paraffin (1)	1 hr 15 min
Paraffin (2)	1 hr 30 min

Table 9. Antibody information and Combination used in FACS

	Antigen	Fluorescence	Clone	Supplier	Cat. #

doi:10.6342/NTU202301366

Stain 1	F4/80	PE-Cy7	BM8	BioLegend	123113
	CD4	PE	RM4-5	BioLegend	100512
	NK1.1	Super bright 600	PK136	eBioscience	63-5941-80
	B220	eF450	RA3-6B2	eBioscience	48-0452-80
	CD3	APC	17A2	eBioscience	100203
	CD62L	FITC	MEL-14	BD bioscience	561917
	CD44	APC-CY7	IM7	BD bioscience	560568
	CD8	PerCp-Cy5.5	53-6.7	BD bioscience	551162
Stain 2	CD11b	PE	M1/70	eBioscience	12-0112-83
	CD11c	PE-Cy7	HL3	BD bioscience	561022
	Gr1	BV570	RB6-8C5	BioLegend	108431

doi:10.6342/NTU202301366

References

1. Shay, J.W. and W.E. Wright, *Telomeres and telomerase: three decades of progress.* Nat Rev Genet, 2019. **20**(5): p. 299-309.
2. Shay, J.W., *Role of Telomeres and Telomerase in Aging and Cancer.* Cancer Discov, 2016. **6**(6): p. 584-93.
3. de Lange, T., *Shelterin: the protein complex that shapes and safeguards human telomeres.* Genes Dev, 2005. **19**(18): p. 2100-10.
4. Harley, C.B., A.B. Futcher, and C.W. Greider, *Telomeres shorten during ageing of human fibroblasts.* Nature, 1990. **345**(6274): p. 458-60.
5. d'Adda di Fagagna, F., et al., *A DNA damage checkpoint response in telomere-initiated senescence.* Nature, 2003. **426**(6963): p. 194-8.
6. Zhang, X., et al., *Telomere shortening and apoptosis in telomerase-inhibited human tumor cells.* Genes Dev, 1999. **13**(18): p. 2388-99.
7. Hemann, M.T. and C.W. Greider, *Wild-derived inbred mouse strains have short telomeres.* Nucleic Acids Res, 2000. **28**(22): p. 4474-8.
8. Kipling, D. and H.J. Cooke, *Hypervariable ultra-long telomeres in mice.* Nature, 1990. **347**(6291): p. 400-2.
9. Morin, G.B., *The human telomere terminal transferase enzyme is a ribonucleoprotein that synthesizes TTAGGG repeats.* Cell, 1989. **59**(3): p. 521-9.
10. Cong, Y.S., W.E. Wright, and J.W. Shay, *Human telomerase and its regulation.* Microbiol Mol Biol Rev, 2002. **66**(3): p. 407-25, table of contents.
11. Rossiello, F., et al., *Telomere dysfunction in ageing and age-related diseases.* Nat Cell Biol, 2022. **24**(2): p. 135-147.
12. Vaiserman, A. and D. Krasnienkov, *Telomere Length as a Marker of Biological Age: State-of-the-Art, Open Issues, and Future Perspectives.* Front Genet, 2020. **11**: p. 630186.
13. Anderson, R., et al., *Length-independent telomere damage drives post-mitotic cardiomyocyte senescence.* EMBO J, 2019. **38**(5).
14. Alder, J.K., et al., *Telomere dysfunction causes alveolar stem cell failure.* Proc Natl Acad Sci U S A, 2015. **112**(16): p. 5099-104.
15. Alder, J.K., et al., *Short telomeres are a risk factor for idiopathic pulmonary fibrosis.* Proc Natl Acad Sci U S A, 2008. **105**(35): p. 13051-6.
16. Chen, R., et al., *Telomerase Deficiency Causes Alveolar Stem Cell Senescence-associated Low-grade Inflammation in Lungs.* J Biol Chem, 2015. **290**(52): p. 30813-29.
17. Kitada, T., et al., *Telomere shortening in chronic liver diseases.* Biochem Biophys Res Commun, 1995. **211**(1): p. 33-9.
18. Hartmann, D., et al., *Telomerase gene mutations are associated with cirrhosis formation.* Hepatology, 2011. **53**(5): p. 1608-17.
19. Rudolph, K.L., et al., *Inhibition of experimental liver cirrhosis in mice by telomerase gene delivery.* Science, 2000. **287**(5456): p. 1253-8.
20. Calado, R.T. and N.S. Young, *Telomere diseases.* N Engl J Med, 2009. **361**(24): p. 2353-65.
21. Martínez, P. and M.A. Blasco, *Telomere-driven diseases and telomere-targeting therapies.* J Cell Biol, 2017. **216**(4): p. 875-887.
22. Sashida, G., et al., *Telomere dynamics in myelodysplastic syndrome determined by telomere measurement of marrow metaphases.* Clin Cancer Res, 2003. **9**(4): p. 1489-96.

doi:10.6342/NTU202301366

23. Colla, S., et al., *Telomere dysfunction drives aberrant hematopoietic differentiation and myelodysplastic syndrome.* Cancer Cell, 2015. **27**(5): p. 644-57.
24. Blasco, M.A., et al., *Telomere shortening and tumor formation by mouse cells lacking telomerase RNA.* Cell, 1997. **91**(1): p. 25-34.
25. Rudolph, K.L., et al., *Longevity, stress response, and cancer in aging telomerase-deficient mice.* Cell, 1999. **96**(5): p. 701-12.
26. Rudolph, K.L., et al., *Longevity, Stress Response, and Cancer in Aging Telomerase-Deficient Mice.* Cell, 1999. **96**(5): p. 701-712.
27. Lee, H.W., et al., *Essential role of mouse telomerase in highly proliferative organs.* Nature, 1998. **392**(6676): p. 569-74.
28. Mohr, U. and I. International Life Sciences, *Pathobiology of the aging mouse*. 1996, Washington, D.C: ILSI. xvi,505p. : ill.
29. Lowe, J.S. and P.G. Anderson, *Stevens and Lowe's human histology*. Fourth edition. ed. 2015, Philadelphia, PA: Elsevier/Mosby.
30. Herrera, E., et al., *Disease states associated with telomerase deficiency appear earlier in mice with short telomeres.* EMBO J, 1999. **18**(11): p. 2950-60.
31. Hemann, M.T., et al., *Telomere dysfunction triggers developmentally regulated germ cell apoptosis.* Mol Biol Cell, 2001. **12**(7): p. 2023-30.
32. Povedano, J.M., et al., *Mice with Pulmonary Fibrosis Driven by Telomere Dysfunction.* Cell Rep, 2015. **12**(2): p. 286-99.
33. Pineiro-Hermida, S., et al., *Telomerase treatment prevents lung profibrotic pathologies associated with physiological aging.* J Cell Biol, 2020. **219**(10).
34. Chen, R., et al., *SPC/ Telomerase Deficiency Causes Alveolar Stem Cell Senescence-associated Low-grade Inflammation in Lungs.* J Biol Chem, 2015. **290**(52): p. 30813-29.
35. Alder, J.K., et al., *Telomere length is a determinant of emphysema susceptibility.* Am J Respir Crit Care Med, 2011. **184**(8): p. 904-12.
36. Liu, T., et al., *Telomerase activity is required for bleomycin-induced pulmonary fibrosis in mice.* J Clin Invest, 2007. **117**(12): p. 3800-9.
37. Elwood, N.J., *Telomere Biology of Human Hematopoietic Stem Cells.* Cancer Control, 2004. **11**(2): p. 77-85.
38. Lansdorp, P.M., *Telomere length and proliferation potential of hematopoietic stem cells.* J Cell Sci, 1995. **108 (Pt 1)**: p. 1-6.
39. Thongon, N., et al., *Hematopoiesis under telomere attrition at the single-cell resolution.* Nat Commun, 2021. **12**(1): p. 6850.
40. Larosa, D.F. and J.S. Orange, *1. Lymphocytes.* J Allergy Clin Immunol, 2008. **121**(2 Suppl): p. S364-9; quiz S412.
41. Townsley, D.M., B. Dumitriu, and N.S. Young, *Bone marrow failure and the telomeropathies.* Blood, 2014. **124**(18): p. 2775-83.
42. Savage, S.A. and B.P. Alter, *The role of telomere biology in bone marrow failure and other disorders.* Mech Ageing Dev, 2008. **129**(1-2): p. 35-47.
43. Calado, R.T. and N.S. Young, *Telomere maintenance and human bone marrow failure.* Blood, 2008. **111**(9): p. 4446-55.
44. Kimura, M., et al., *Synchrony of telomere length among hematopoietic cells.* Exp Hematol, 2010. **38**(10): p. 854-9.
45. Sakaguchi, H., et al., *Peripheral blood lymphocyte telomere length as a predictor of response to immunosuppressive therapy in childhood aplastic anemia.* Haematologica, 2014. **99**(8): p. 1312-6.

doi:10.6342/NTU202301366

46. Guilliams, M., et al., *Dendritic cells, monocytes and macrophages: a unified nomenclature based on ontogeny.* Nat Rev Immunol, 2014. **14**(8): p. 571-8.
47. Quinn, K.M., et al., *Age-Related Decline in Primary CD8(+) T Cell Responses Is Associated with the Development of Senescence in Virtual Memory CD8(+) T Cells.* Cell Rep, 2018. **23**(12): p. 3512-3524.
48. Daniil, Z., et al., *CD8+ T lymphocytes in lung tissue from patients with idiopathic pulmonary fibrosis.* Respir Res, 2005. **6**(1): p. 81.
49. Shao, L., et al., *Telomere Dysfunction in Peripheral Lymphocytes as a Potential Predisposition Factor for Renal Cancer.* The Journal of Urology, 2007. **178**(4): p. 1492-1496.
50. Kroupa, M., et al., *Telomere length in peripheral blood lymphocytes related to genetic variation in telomerase, prognosis and clinicopathological features in breast cancer patients.* Mutagenesis, 2020. **35**(6): p. 491-497.
51. Chakravarti, D., et al., *Telomere dysfunction activates YAP1 to drive tissue inflammation.* Nat Commun, 2020. **11**(1): p. 4766.
52. Yang, T.L.B., et al., *Mutual reinforcement between telomere capping and canonical Wnt signalling in the intestinal stem cell niche.* Nature Communications, 2017. **8**.
53. Liu, Y.Y., et al., *Telomere shortening activates TGF-beta/Smads signaling in lungs and enhances both lipopolysaccharide and bleomycin-induced pulmonary fibrosis.* Acta Pharmacol Sin, 2018. **39**(11): p. 1735-1745.
54. Zhang, K., L. Xu, and Y.S. Cong, *Telomere Dysfunction in Idiopathic Pulmonary Fibrosis.* Front Med (Lausanne), 2021. **8**: p. 739810.
55. Blasco, M.A., et al., *Functional characterization and developmental regulation of mouse telomerase RNA.* Science, 1995. **269**(5228): p. 1267-70.
56. Clevers, H., *Searching for adult stem cells in the intestine.* EMBO Molecular Medicine, 2009. **1**(5): p. 255-259.

doi:10.6342/NTU202301366